Bioengineered ncRNAs selectively change cellular miRNome profiles for cancer therapy

Pui Yan Ho, Zhijian Duan, Neelu Batra, Joseph L. Jilek, Mei-Juan Tu, Jing-Xin Qiu, Zihua Hu, Theodore Wun, Primo N. Lara, Ralph W. DeVere White, Hong-Wu Chen, Ai-Ming Yu*

Department of Biochemistry & Molecular Medicine, UC Davis School of Medicine, Sacramento, CA 95817, USA (PYH, ZJD, NB, JJL, MJT, HWC, AMY); Department of Pathology, Roswell Park Cancer Institute, Buffalo, NY 14263, USA (JXQ); Center for Computational Research, New York State Center of Excellence in Bioinformatics & Life Sciences, State University of New York at Buffalo, Buffalo, NY 14260, USA (ZH); Division of Hematology Oncology (TW), Department of Internal Medicine (PNL), Department of Urology (RWDW), UC Davis School of Medicine, Sacramento, CA 95817, USA

JPET Fast Forward. Published on March 30, 2018 as DOI: 10.1124/jpet.118.247775
This article has not been copyedited and formatted. The final version may differ from this version.

Running Title: Bioengineered ncRNAs for cancer therapy

Address correspondence to: Prof. Ai-Ming Yu, Department of Biochemistry & Molecular Medicine, UC Davis School of Medicine, Sacramento, CA 95817, USA; Email: aimyu@ucdavis.edu.

Number of text pages: 26

Number of tables: 1

Number of figures: 6

Number of references: 53

Number of words in the Abstract: 250

Number of words in the Introduction: 630

Number of words in the Discussion: 1,353

Abbreviations: ncRNA, noncoding RNA; nCAR, ncRNA carrier; RNAi, RNA interference; tRNA, transfer RNA; miRNA, microRNA; siRNA, small interfering RNA; sRNA, small RNA; FPLC, fast protein liquid chromatography; HPLC, high performance liquid chromatography; cMET, tyrosine-protein kinase Met; CDK6, cyclin dependent kinase 6; SIRT1, sirtuin 1; STAT3, signal transducer and activator of transcription 3; ABCC4, ATP binding cassette subfamily C member 4; BERA, bioengineered RNA agent.

JPET Fast Forward. Published on March 30, 2018 as DOI: 10.1124/jpet.118.247775
This article has not been copyedited and formatted. The final version may differ from this version.

ABSTRACT

Noncoding RNAs (ncRNAs) produced in live cells may better reflect intracellular ncRNAs for research and therapy. Attempts were made to produce biological ncRNAs, but at low yield or success rate. Here we first report a new ncRNA bioengineering technology, using more stable ncRNA carrier (nCAR) containing a pre-miR-34a derivative identified by rational design and experimental validation. This approach offered a remarkable higher-level expression (40-80% of total RNAs) of recombinant ncRNAs in bacteria, and gave an 80% success rate (33 out of 42 ncRNAs). New FPLC and spin-column based methods were also developed for large- and small-scale purification of milligrams and micrograms of recombinant ncRNAs from half liter and milliliters of bacterial culture, respectively. We then used two bioengineered nCAR/miRNAs to demonstrate the selective release of target miRNAs into human cells, which were revealed to be Dicer dependent (miR-34a-5p) or independent (miR-124a-3p), and subsequent changes of miRNome and transcriptome profiles. MiRNA enrichment analyses of altered transcriptome confirmed the specificity of nCAR/miRNAs in target gene regulation. Furthermore, nCAR assembled miR-34a-5p and miR-124-3p were active in suppressing human lung carcinoma cell proliferation through modulation of target gene expression (e.g., cMET and CDK6 for miR-34a-5p; STAT3 and ABCC4 for miR-124-3p). In addition, bioengineered miRNA molecules were effective in controlling metastatic lung xenograft progression, as demonstrated by live animal and *ex vivo* lung tissue bioluminescent imaging as well as histopathological examination. This novel ncRNA bioengineering platform can be easily adapted to produce various ncRNA molecules, and biologic ncRNAs hold the promise as new cancer therapeutics.

JPET Fast Forward. Published on March 30, 2018 as DOI: 10.1124/jpet.118.247775
This article has not been copyedited and formatted. The final version may differ from this version.

INTRODUCTION

Noncoding RNAs such as miRNAs play important roles in the regulation of target gene expression underlying various cellular processes, and dysregulation of ncRNAs is highly associated with human diseases including cancer (Cech and Steitz, 2014; Rupaimoole and Slack, 2017; Thyagarajan et al., 2018). While the actions of ncRNAs have been extensively studied, our knowledge might not fully encompass these molecules on a true biological level. NcRNAs currently used for biomedical research are produced primarily by chemical synthesis and decorated extensively with a wide array of artificial modifications (Corey, 2007; Bramsen and Kjems, 2012; Khvorova and Watts, 2017). Such chemically-engineered/synthesized ncRNA agents from different manufacturers and laboratories vary broadly in the types, sites and degrees of artificial modifications, and thus likely have distinct higher-order structures, physicochemical properties, biological/pharmacological activities and safety profiles. Therefore, chemo-engineered ncRNA molecules may not represent the properties of natural ncRNAs produced within live cells (Ho and Yu, 2016; Pereira et al., 2017). Recognized as foreign invaders by specific factors such as toll-like receptors (Hornung et al., 2005; Robbins et al., 2009), synthetic ncRNAs have been well documented to cause off-target effects and induce immunogenicity, which also vary broadly with different chemical modifications. The recent termination of Phase I clinical study on synthetic miR-34a mimic (MRX34) (Beg et al., 2017), owing to high incidence of adverse immune responses, again testifies the body's capability to distinguish chemo-engineered RNAi agents as foreign. Therefore, biological approaches such as *in vitro* transcription (Beckert and Masquida, 2011) and especially, bioengineering in live cells (Ponchon and Dardel, 2007; Ponchon et al., 2009; Huang et al., 2013; Li et al., 2014; Chen et al., 2015; Li et al., 2015; Wang et al., 2015; Pereira et al., 2016; Fang et al., 2017; Li et al., 2018), are highly warranted to produce natural RNA molecules that should better represent

JPET Fast Forward. Published on March 30, 2018 as DOI: 10.1124/jpet.118.247775
This article has not been copyedited and formatted. The final version may differ from this version.

cellular ncRNA properties for basic research and experimental therapy (Ho and Yu, 2016; Pereira et al., 2017).

Efforts have been made to produce biological ncRNAs via fermentation, whereas at a low yield or success rate. The use of p19 RNA-binding protein (Huang et al., 2013) offers a way to produce fully-processed siRNAs in *E. coli*; however, the low yield (e.g., 10-80 μg per liter bacterial culture) makes this method impractical for the production of milligram quantities of RNAi agents. Utilization of tRNA scaffold (Ponchon and Dardel, 2007; Ponchon et al., 2009) may facilitate large-scale (e.g., up to 20 mg per liter fermentation) production of ncRNAs; nevertheless, adoption of this method revealed that less than 20% of target ncRNAs could actually be expressed at isolatable levels (e.g., >3% of total RNAs) (Chen et al., 2015). Our recent efforts to produce recombinant pre-miRNA (mir) have demonstrated ample expression (10-20% of total RNAs) of a hybrid ncRNA molecule in *E. coli*, namely pre-miR-34a and $tRNA^{Met}$ fused Sephadex aptamer (MSA) (MSA/mir-34a) (Chen et al., 2015). Although MSA/mir-34a can be used as a versatile scaffold, the success rate for producing isolatable target ncRNAs is still less than 30%, and the dependence on Sephadex aptamer is unknown.

Here, we first report the development of a more stable and reliable ncRNA carrier (nCAR) for rapid production of milligrams of target ncRNA agents at an enormously higher expression level (40-80% of total RNAs) and success rate (~80%; 33 out of 42 target ncRNAs). We further established a readily adaptable pipeline for both small- and large-scale production of bioengineered ncRNAs, which we applied to generate a collection of ready-to-use biologic ncRNA molecules. Using two nCAR/miRNAs as examples, we further demonstrate that bioengineered miRNA agents, with intrinsic RNA properties for specific processing to target miRNAs, were able to selectively rewrite miRNome profiles and alter transcriptome of human

JPET Fast Forward. Published on March 30, 2018 as DOI: 10.1124/jpet.118.247775
This article has not been copyedited and formatted. The final version may differ from this version.

cells, leading to antiproliferative properties against human lung carcinoma cells *in vitro* and antitumor activities in xenograft mouse models *in vivo*.

JPET Fast Forward. Published on March 30, 2018 as DOI: 10.1124/jpet.118.247775
This article has not been copyedited and formatted. The final version may differ from this version.

MATERIALS AND METHODS

Bacterial culture. DH5α (Thermo Fisher Scientific, Rockford, IL) and HST08 (Clontech Laboratories, Mountain View, CA) were grown at 37°C in LB supplemented with 100 μg/ml ampicillin for plasmid preparation and amplification. To produce RNA, 2×YT media supplemented with 100 μg/ml ampicillin was used for enriched growth of HST08 *E. coli*.

Human cell culture. Human lung carcinoma cell lines A549 H23, H1650, H1299 and H1975 were purchased from American Type Culture Collection (Manassas, VA, USA). HEK293T and Dicer-KO (4-25) cell lines were kindly provided by Prof. Bryan R. Cullen (Duke University, Durham, NC) (Bogerd et al., 2014). Luciferase and GFP-expressing A549-Luc-GFP cells were generated by transduction with pCCLc-Luc-EGFP lentiviral constructs (Vector Core, UC Davis Medical Center, Sacramento, CA). Lung carcinoma cell lines were maintained in RPMI 1640 supplemented with 10% fetal bovine serum and 293T cells were maintained in DMEM supplemented with 10% fetal bovine serum and Gentamicin (10 μg/mL), both grown at 37°C in a humidified atmosphere with 5% CO_2 and 95% air.

Construction of ncRNA expression plasmids. Sequences of individual miRNAs and pre-miR-34a were obtained from miRBase (http://www.mirbase.org/), while siRNA and RNA aptamer sequences were gathered from previously reported studies (Supplemental Table S1). Inserts coding target ncRNA sequences (Supplemental Table S2) were generated by PCR amplification using primers (IDT, San Diego, CA) (Supplemental Table S2). Amplicons were annealed into pBSTNAV (Ponchon et al., 2009) linearized by *SacII* and *EagI* (New England Biolabs, Ipswich, MA) via Seamless Recombination (Clontech Laboratories). Plasmids were propagated in DH5α cells and confirmed by sequencing analyses (Genscript, Piscataway, NJ).

Expression of recombinant RNAs in *E. coli.* HST08 competent cells were transformed with target plasmids and then grown either on small scale (5-50 mL) or large scale (500-600 mL). Total RNAs were isolated by phenol extraction, quantitated with a NanoDrop 2000 Spectrophotometer (Thermo Fisher Scientific, Rockford, IL), and analyzed by denaturing urea (8 M) polyacrylamide (8%) gel electrophoresis (PAGE). Images were acquired with ChemiDoc MP Imaging System (Bio-Rad, Hercules, CA). Band intensities were used to roughly estimate target RNA expression relative to total RNAs. Precise calculation of the fraction of target RNA in total RNAs was achieved by dividing the area of target RNA peak by total areas of all peaks in chromatograph during FPLC purification, as shown below.

Small- and large-scale purification of nCAR/sRNAs. Target BERA was purified on small scale using spin columns: RNA Clean & Concentrator and Select-a-Size DNA Clean & Concentrator (Zymo Research, Irvine, CA). RNA was isolated following the protocols suggested for >200 nt (RNA Clean & Concentrator) sequentially followed by a 50 bp cutoff protocol (Select-a-Size DNA Clean & Concentrator). Large-scale purification of target BERA was performed with a NGC QUEST 10PLUS fast protein liquid chromatography system (Bio-Rad) equipped with an anion exchange Enrich-Q 10×100 column (Bio-Rad). Separation of nCAR/sRNA from total RNAs was achieved on an Enrich-Q 10×100 column that was first equilibrated with Buffer A (10 mM sodium phosphate, pH 7.0) at a constant flow rate of 2.5 ml/min for 2 min and then followed by a gradient elution at the same flow rate: 55% Buffer B (Buffer A + 1 M sodium chloride, pH 7.0) for 4.8 min, 55-75% Buffer B for 20.4 min, and then 100% Buffer B for 9.6 min. FPLC traces were monitored at 260/280 nm using a UV/Vis detector and individual fractions were collected for urea-PAGE analyses. After confirmation of purity and expected size, fractions containing target BERA were pooled, precipitated by ethanol, desalted and concentrated/dissolved in

nuclease-free water with an Amicon ultra-2mL centrifugal filter (30 kDa; EMD Millipore, Billerica, MA).

Determination of RNA purity. RNA purity was quantitated by HPLC analysis as previously described (Wang et al., 2015) and endotoxin activity was determined using the Pyrogent-5000 kinetic LAL assay (Lonza, Walkersville, MD) by following manufacturer's instructions, prior to *in vitro* and *in vivo* functional studies. The majority of nCAR/sRNAs purified by FPLC were >98% pure (Table 1) with minimal endotoxin levels (<1 EU/μg RNA).

RNA sequencing and data analyses. 293T and Dicer-KO cells were transfected with 20 nM of nCAR/miR-34a-5p, nCAR/miR-124-3p or control tRNA. Cells were treated in triplicate and processed and sequenced separately. Total RNAs were isolated using TRIzol-chloroform protocol (Abcam) at 48 hr post-transfection and RNA integrity was assessed by 1% standard agarose gel electrophoresis.

Small RNAs: Library construction was prepared by BGI, where small RNAs less than 30 nt were collected through gel separation (15% Urea-PAGE) starting with 1 μg of total RNA. Small RNA fragments were ligated to adenylated 3' adapters annealed to unique barcodes, followed by the ligation of 5' adapters and reverse transcription (RT). After synthesis of the first strand cDNA, the product was expanded by 15 cycles of PCR amplification. A second size selection operation was carried out to purify the PCR amplicons from nonspecific products, selecting 103–115 bp fragments by gel separation. After gel purification, PCR yield was quantified by Qubit 3.0 Fluorometer (Invitrogen, Carlsbad, CA) and samples were pooled to make a single strand DNA circle (ssDNA circle) to yield the final small RNA library. DNA nanoballs (DNBs) were generated with the ssDNA circle by rolling circle replication (RCR) to enlarge fluorescent signals at the sequencing process. The DNBs were loaded into the patterned nanoarrays and single-end

reads of 50 bp were read on the BGISEQ-500 platform (Shenzhen, China). The FASTQ-formatted sequence data were analyzed using the miRDeep module (An et al., 2013) to obtain the read counts of known miRNAs. To compute the read counts derived from transfected nCAR/miR-34a-5p or nCAR/miR-124-3p, a PERL script was developed to map sequence reads from FASTQ-formatted sequence data to the corresponding constructor, followed by counting isoform reads in individual samples. Read counts of known miRNAs and sRNAs derived from nCAR/miR-34a-5p or nCAR/miR-124-3p among individual samples were thus used for the analysis of significantly, differentially expressed miRNAs ($P < 0.05$ and $\log_2CPM > 6$) between phenotype using EdgeR (Robinson et al., 2010).

Messenger RNAs: mRNAs were purified using poly-T oligo-attached magnetic beads. Following purification, the mRNA was fragmented into small pieces using divalent cations under elevated temperature. The cleaved RNA fragments were copied into first strand cDNA using random primers by reverse transcription, followed by second strand cDNA synthesis using DNA Polymerase I and RNase H. These cDNA fragments contain an additional 'A' at the 3' end to allow subsequent ligation of the adapter. The products were then purified and enriched with PCR amplification, quantified with Qubit and used to create DNB-based nanoarrays by RCR. Stepwise sequencing was performed using the combinatorial Probe-Anchor (cPAL) ligation approach and read on the BGISEQ-500 system. The FASTQ-formatted sequence data were analyzed using a BWA-RSEM-EdgeR workflow (Li and Durbin, 2009; Robinson et al., 2010; Li and Dewey, 2011), with sequence reads mapped to the reference human-genome assembly (Feb. 2009, GRCh37/hg19) with BWA software. Sequence read counts for individual genes were computed using RSEM, and the resulting read counts from individual samples were subjected to the detection of differentially expressed mRNAs ($\log_2FC > 1.2$ or $\log_2FC < 0.8$, $P < 0.05$, and $\log_2CPM > 5$) between phenotypes using EdgeR package. Networks, functions, and pathways analyses were generated using Ingenuity Pathway Analysis (Ingenuity Systems;

Qiagen, Redwood City, CA), primarily based on experimentally demonstrated interactions in human and rodent studies.

Enrichment analysis. miRNA target enrichment analyses of significantly downregulated genes ($\log_2$FC < 0.8, P < 0.05, and $\log_2$CPM > 5) were undertaken using miRNA targets predicted by TargetScan (Lewis et al., 2005), and enrichment P-values were computed by Fisher's exact test.

Reverse transcription quantitative real-time PCR. Cells were transfected with 20 nM of nCAR/miR-34a, nCAR/miR-124, or control using Lipofectamine 3000 (Life Technologies, Carlsbad, CA) and harvested at 48 h post transfection. Total RNAs were extracted using Direct-zol RNA isolation kit (Zymo Research) and 500 ng of total RNAs were used for cDNA synthesis with random hexamers or respective stem-loop primers (Supplemental Table S3). RT was conducted with NxGen M-MuLV reverse transcriptase (Lucigen, Middleton, WI), and qPCR analysis was carried out on a CFX96 Touch real-time PCR system (Bio-Rad) using quantitative RT-PCR master mix and respective primers (Supplemental Table S3). Levels of miRNA were normalized to U6 snRNA and levels of mRNA were normalized to 18S rRNA (N = 9) in corresponding samples, determined using the formula $2^{-\Delta\Delta CT}$. Reactions were run in triplicate in three independent experiments and similar results were obtained.

Cell viability assay. Cells were transfected with various doses of nCAR/miR-34a-5p, nCAR/miR-124-3p, or control tRNA. Cell viability was determined with CellTiter-Glo 2.0 assay kit (Promega, Madison, WI) at 72 post-transfection, according to manufacturer’s protocol. Luminescence was recorded using a SpectraMax Microplate Reader (Molecular Devices, Sunnyvale, CA) at an integration time of 250 ms. Inhibition was calculated by adjusting vehicle control to 0% and dose response curves were established by plotting inhibition versus RNA concentration. Data were fit into a normalized inhibitory dose-response model with variable

JPET Fast Forward. Published on March 30, 2018 as DOI: 10.1124/jpet.118.247775
This article has not been copyedited and formatted. The final version may differ from this version.

slope (Y = 100/(1+10^((LogEC50-X)*HillSlope))); GraphPad Prism, San Diego, CA) for the estimation of EC50 and Hill slope values (Supplemental Table S4). All experiments were performed in triplicates.

Western blot assay. A549, 293T, and Dicer-KO 293T cells were seeded at 0.25×10^6 cells/well and treated with 30 nM nCAR/miR-34a-5p, nCAR/miR-124-3p, or tRNA control. Cultured cells were harvested at 48 h and lysed with RIPA lysis buffer (Sigma Aldrich, St. Louis, MO) containing protease inhibitor cocktail (Roche Diagnostics, Mannheim, Germany). Total cell lysate (30 μg) was resolved by 10% SDS-PAGE gel, transferred to PVDF membranes (250 mA for 2 hours), and probed with target antibodies. Antibodies against CDK6 (C-21), cMET (C-28), Dicer (H-212), GAPDH (FL-335) and SIRT1 (H-300) were obtained from Santa Cruz Biotechnology (Santa Cruz, CA), p-STAT3 (Tyr705) and STAT3 (124H6) were acquired from Cell Signaling Technology (Beverly, MA), β-actin (AC-15) from Sigma-Aldrich (St Louis, MO) and MRP4 (M4I-10) from Abcam (Cambridge, MA). Subsequently, secondary antibodies linked with peroxidase were anti-rabbit (Jackson ImmunoResearch Inc., West Grove, PA), anti-mouse IgG or anti-rat IgG (Cell Signaling). Protein bands were captured by a luminescent image analyzer (ChemiDoc MP Imaging System).

Metastatic lung xenograft mouse models and therapy studies. All animal procedures were approved by the Institutional Animal Care and Use Committee of University of California, Davis, and all animal studies were conducted in accordance with the relevant national and international guidelines. Five week old female non-obese diabetic/severe combined immunodeficient (NOD/SCID) mice (NOD.CB17-Prkdcscid/J) were purchased from Jackson Laboratory and adaptively fed at least one week before experiments.

A549 metastatic xenograft mouse models were established by injecting 3.5×10^6 A549-luc/GFP cells via tail vein. Tumor growth was monitored using bioluminescence imaging by injecting D-luciferin potassium salt solution (150 mg/kg) intraperitoneally 10 min post-anesthesia. Images were acquired with the ChemiDoc MP Imaging System. 14 days after inoculation, 27 mice were randomly divided into 3 three groups (N = 9 per group). Mice were treated intravenously with 30 μg of control tRNA, nCAR/miR-34a-5p or nCAR/miR-124-3p, formulated with in vivo-jetPEI (Polyplus Transfection), three times per week for three weeks. At the end of the study, all mice were sacrificed and lungs were dissected, weighed, and imaged *ex vivo* for GFP signals. Lung tissues were further fixed with 10% formalin and subjected to hematoxylin and eosin (H&E) staining for histopathological evaluation in the Histology Facility at Roswell Park Cancer Institute (Buffalo, NY, USA). H&E-staining images (100×) were captured using an Olympus camera (DP25) and CellSens software (Olympus, Center Valley, PA).

Induction of cytokine release. Female BALB/c mice at five to six weeks of age (Jackson Laboratory) were administered intravenously via tail vein with 30 μg of in vivo-jetPEI-formulated control tRNA, nCAR/miR-34a-5p or nCAR/miR-124-3p. Separate groups of animals without any treatment or treated intravenously with 20 μg of lipopolysaccharide (LPS) were used as controls. Blood was collected 1 h after administration and serum was isolated for the quantification of cytokine IL-6 and TNFα levels using mouse ELISA assay kits (Thermo Fisher Scientific).

Statistical analysis. Data are presented as mean ± SD. Statistics analysis was performed using unpaired Student's *t*-test, one-way ANOVA, or two-way ANOVA (GraphPad Prism, San Diego, CA). $P < 0.05$ was considered to be statistically significant.

RESULTS

Identification of pre-miR-34a G138U/139ΔG derivative for ncRNA carrier. To enable heterogeneous expression of recombinant ncRNAs in bacteria, we sought to assess the foundational basis for chimeric ncRNA design. We first found that $tRNA^{Met}$ standalone showed no obvious expression in *E. coli* (Fig. 1A). In sharp contrast, $tRNA^{Met}$ fused Sephadex aptamer (MSA) was overexpressed, indicating the importance of Sephadex aptamer for accumulation of the chimera (Fig. 1B). Furthermore, human pre-miR-34a itself was noticeably expressed in bacteria (≤ 2% of total RNAs) and hybrid MSA/mir-34a showed an improved accumulation (10-20% of total RNAs) (Fig. 1C), demonstrating the stabilities of pre-miR-34a and chimeric ncRNA for the success of heterogeneous expression.

Therefore, we aimed at refining pre-miR-34a to achieve a more stable and higher level of expression, and assessed the dependence on Sephadex aptamer. Our approach was to use pre-miR-34a (110 nt) and rationally modify small bulges and kinks to yield more stable stems (Fig. 1D), which might lead to greater degree of RNA stability and accumulation in the host. Among five pre-miR-34a derivatives evaluated experimentally, we found that construct G138U/139ΔG showed the highest level of expression (>50% of total RNAs), which was also independent of Sephadex aptamer (Fig. 1D). Supporting this observation, the positional entropy of pre-miR-34a G138U/139ΔG was 4.6 Kcal/mol lower than its wild type counterpart (tRNA/mir-34a-110nt). In addition, the increased expression of tRNA-fused pre-miR-34a G138U/139ΔG derivative, as compared to MSA/pre-miR-34a (Chen et al., 2015), was shown in both HST08 and Top10 common *E. coli* stains (Supplemental Fig. 1). As a result, the pre-miR-34a G138U/139ΔG derivative was selected to fuse to a tRNA (e.g., $tRNA^{Met}$) as ncRNA carrier (nCAR) for bioengineering RNAi agents.

nCAR permits a remarkable high-level production of target ncRNAs at a high success rate. The nCAR was applied for the assembly of target RNAi agents, where small RNAs (sRNAs) such as miRNAs, siRNAs and aptamers substituted miR-34a sequences or were directly added to designated locations (Fig. 2A). Considering the 5' counting rule (Park et al., 2011), a total of 42 nCAR/sRNA agents were designed (Supplemental Tables 1 and 2). The coding sequences of individual target bioengineered ncRNA agents (BERA) were thus cloned into a target vector (Supplemental Fig. 2). Following transformation and fermentation, we assessed the expression of target BERAs by urea-PAGE analysis of total RNAs isolated from *E. coli*. Excitingly, we found that 33 BERAs were successfully expressed at a remarkably high level (40-80% of total RNAs; Fig. 2B), which gave a success rate of 80% (33 out of 42 target ncRNAs). The results demonstrate the robustness of nCAR for an improved higher level, heterogeneous expression of target RNAi agents.

On-demand small- and large-scale purification of bioengineered ncRNAs. We next sought for methods to isolate target BERAs from total RNAs. While the utility of the nCAR platform is purposed for large-scale production of milligrams of BERAs, we did examine the practicality of purifying microgram quantities that may be used for initial or high-throughput screening. Since the nCAR system generally offers BERAs (e.g., nCAR/miR-34a-5p and nCAR/miR-124-3p, etc.) around a length of 180 nt, we assessed whether target BERAs could be isolated with commercially available Select-a-Size DNA Clean & Concentrator (Fig. 2C) based on similar physicochemical properties of nucleic acids. The 50-bp selection was able to produce >88% pure BERA (determined by HPLC method) with a yield of 15-20 μg/ml culture (Supplemental Table 3). When used in combination with the RNA Clean & Concentrator spin columns that remove large RNAs (Fig. 2C), the purity of isolated BERAs was over 97% (Supplemental Table 3). Although the two-column method unsurprisingly offered a lower yield than the single-column,

overall yield (~14 μg/ml culture or 30-40% of total RNAs) was still tremendously high, owing to the remarkable high-level expression.

To achieve large-scale purification, we established a new anion exchange FPLC method. Up to 15 mg of total RNAs were loaded onto an Enrich-Q 10×100 column and separated by a single-run, salt-gradient elution (Fig. 2C). The majority of FPLC-isolated BERAs displayed a high degree of homogeneity (>98%; Table 1), as determined by HPLC method (Supplemental Fig. 3). Given such enhanced expression and purification yield, we readily obtained up to 10 mg of target BERAs in a single run and 4-20 mg of pure BERAs from 1 L bacterial fermentation (Table 1). In addition, endotoxin was flushed through this process and the endotoxin activities of final BERAs were minimal (e.g., nCAR/miR-34a-5p: 0.85 EU/μg RNA; nCAR/miR-124-3p: 0.1 EU/μg RNA), which are much lower than the reported levels (2,000 EU/μg DNA) to induce cytotoxicity (Butash et al., 2000) and that (≤ 5 EU/mg of body weight at a rate of 30 μg RNA/h; see the following animal studies) recommended for mouse studies (Malyala and Singh, 2008), and thus ensure endotoxin-free BERAs for functional studies.

Selective release of target miRNAs from bioengineered ncRNAs in human cells rewrites miRNome, dependent (miR-34a-5p) or independent (miR-124-3p) on endoribonuclease Dicer. To examine whether target miRNAs can be specifically generated from BERAs in human cells and whether this process is Dicer dependent, we conducted a small RNA sequencing study on human 293T cells and Dicer-knockout (Dicer-KO) counterparts (Bogerd et al., 2014) treated with nCAR/miR-34a-5p, nCAR/miR-124-3p, and control RNA. The result showed that nCAR/miR-34a-5p was selectively processed to miR-34a-5p as its dominant isoform (22-nt; starting site 0) in 293T cells, as well as to lower reads of other isoforms (Fig. 3A). However, miR-34a-5p levels were 27-fold lower in Dicer-KO 293T cells than wild type 293T cells,

demonstrating a critical role for Dicer in the production of miR-34a-5p from nCAR/miR-34a-5p. Surprisingly, nCAR/miR-124-3p was mainly processed to a 23-nt isoform starting at position 0 in wild type 293T cells whereas a 22-nt specie from position +1 in Dicer-KO cells. Since miR-124-3p naturally exists as 20-nt, additional nucleotides carried over from pre-miR-34a at the 3' end of the carrier indicates a unique cleavage of nCAR/miR-124-3p to offer miR-124-3p. Most interestingly, comparable levels of miR-124-3p were generated from nCAR/miR-124-3p in wild type and Dicer-KO 293T cells (Fig. 3A), indicating the independence of Dicer for the production of miR-124-3p.

The selective release of target miR-34a-5p from nCAR/miR-34a-5p in human cells led to a specific change of miRNome profiles, where miR-34a-5p became the most abundant miRNA in both wild type 293T cells (>16 million reads of all miRNAs) and Dicer-KO cells (<0.5 million of reads) (Fig. 3B). Likewise, miR-124-3p became the seventh-most and most abundant miRNA in wild type and Dicer-KO 293T cells, respectively, post treatment with nCAR-miR-124-3p. The increase in target miRNA levels among miRNome was further confirmed by qPCR analyses (Supplemental Fig. 4A). Although the fold of increase in miR-34a-5p levels was "surprisingly" higher in the Dicer-KO cells than wild type 293T cells, this scenario is simply attributable to the low basal expression level of miR-34a-5p in Dicer-KO cells (Fig. 3A). Together, our results demonstrate that a large number of target miRNAs can be selectively generated from BERAs in human cells, in a Dicer dependent (e.g., miR-34a-5p) or independent (e.g., miR-124-3p) manner, which subsequently rewrites cellular miRNome profiles.

Bioengineered miRNAs specifically modulate the transcriptome profiles in human cells. To delineate the effects of BERA on miRNA target gene expression and assess its specificity, we processed the same set of RNA samples for mRNA sequencing study. The results showed that 112 genes were significantly downregulated and 193 upregulated in nCAR/miR-34a-treated

JPET Fast Forward. Published on March 30, 2018 as DOI: 10.1124/jpet.118.247775
This article has not been copyedited and formatted. The final version may differ from this version.

293T cells, as well as 260 genes downregulated and 290 upregulated in nCAR/miR-124-treated 293T cells (Fig. 4A). These downregulated genes include many well-documented targets for specific miRNA (e.g., AMER1, GAS1, and NECTIN1 for miR-34a; VAMP3, SNAI2, IQGAP1, TMEM109, and RHOG for miR-124) (Chang et al., 2007; Karginov et al., 2007; Chi et al., 2009; Kaller et al., 2011), as well as some genes that have not been reported before (e.g., BAG2 and BCL6B for miR-34a; NID1 and VIM for miR-124). The suppression of several transcripts was further verified by qPCR analyses (Supplemental Fig. 4B) with gene selective primers (Supplemental Table 4), where housekeeping gene levels were not altered (Supplemental Fig. 4C).

On the other hand, only six genes were significantly downregulated in Dicer-KO 293T cells by nCAR/miR-34a-5p (Fig. 4B), which have not been connected to miR-34a, again supporting the dependence on Dicer for miR-34a-5p production as well as the selectivity of nCAR/miR-34a-5p in the regulation of miR-34a target gene expression. In sharp contrast, nCAR/miR-124-3p significantly reduced the expression of 68 genes in Dicer-KO cells, among which many (e.g., VAMP3, SNAI2, and RHOG) are known miR-124 targets and show good overlap with targets identified in wild type 293T cells (Fig. 4B). This is in agreement with the independence on Dicer in generating comparable high levels of miR-124-3p isoforms from nCAR/miR-124-3p in cells, whereas the major isoforms differed in length and position.

The selectivity of nCAR/miRNA in the regulation of miRNA target gene expression was further demonstrated by miRNA enrichment analyses. MiR-34a-5p was highly enriched from nCAR/miR-34a-5p-downregulated genes in 293T cells while the same did not hold true for Dicer KO cells (Fig. 4C), interweaving the specific effects on target gene expression due to Dicer-dependent excision of miR-34a-5p from nCAR/miR-34a-5p. Unsurprisingly, miR-449/34c within the same miR-34/449 family was also enriched from nCAR/miR-34a-5p-downregulated genes in

JPET Fast Forward. Published on March 30, 2018 as DOI: 10.1124/jpet.118.247775
This article has not been copyedited and formatted. The final version may differ from this version.

293T cells, supporting the similarity of their functions in gene regulation. However, miR-449/34c showed a low abundance ($log_2CPM < 6$) and/or no significant ($P > 0.05$) change in its expression after BERA treatment, and thus unlikely had any contribution to the change of transcriptome. Interestingly, miR-124-3p was highly enriched for nCAR/miR-124-3p-downregulated genes in both wild type and Dicer-KO 293T cells (Fig. 4C), which not only supports the selectivity of nCAR/miR-124-3p in the regulation of miR-124 target gene expression but also demonstrates the independence of miR-124-3p formation on Dicer. Likewise, miR-506 within the miR-124/506 family was enriched, although miR-506 was absent (0 reads) in all genotype and treatment cells. Additionally, we employed ingenuity pathway analysis to investigate the biological pathways affected by BERA-downregulated genes. Gene regulation networks regulated by miR-34a were linked to cell growth, DNA replication, and cell proliferation and survival, while miR-124 was associated with cell morphology, maintenance, and gene expression (Fig. 4D). Taken together, these results demonstrate that nCAR/miRNAs displayed a high selectivity in gene regulation in human cells.

Biologic miRNAs reduce the protein levels of target genes in human cells. We further chose a few well-established targets for miR-34a (e.g., CDK6 and SIRT1) (Sun et al., 2008; Yamakuchi et al., 2008) and miR-124 (e.g., STAT3 and ABCC4/MRP4) (Hatziapostolou et al., 2011; Markova and Kroetz, 2014) to delineate the impact of bioengineered miRNAs on protein expression levels. Immunoblot analyses revealed a consistent suppression of CDK6 and SIRT1 protein levels by nCAR/miR-34a-5p in 293T cells (Supplemental Fig. 5A), as a result of high levels of released miR-34a-5p (Fig. 3A) However, in Dicer-KO cells, CDK6 protein levels were unchanged while SIRT1 levels were steadily reduced by nCAR/miR-34a-5p, which could be due to a much lower level of miR-34a-5p produced in the absence of Dicer (Fig. 3A). This interesting observation might also indicate distinct sensitivities of different targets to the absolute amounts or extents of change of cellular miR-34a levels (Fig. 3A). Similarly, variable degrees of impact of

nCAR/miR-124-3p on the protein levels of miR-124-3p targeted STAT3 and MRP4/ABCC4 (Supplemental Fig. 5B) were identified in wild type and Dicer-KO 293T cells, which might be attributable to the difference in the most abundant miR-124-3p isoforms produced in those cells (Fig. 3A) with slightly-altered seed sequences or nucleotides.

Bioengineered nCAR/miR-34a-5p and miR-124-3p are active in suppressing human lung carcinoma cell proliferation *in vitro*. To further evaluate the utility of BERAs, we investigated the dose-dependent anti-proliferation activities of two model BERAs, nCAR/miR-34a-5p and nCAR/miR-124-3p, against a variety of human lung carcinoma cells with different p53 and EGFR status as lung cancer remains the most lethal cancer in the United States (Siegel et al., 2017), and restoration of miR-34a and miR-124 expression or function is effective to inhibit lung cancer cell growth (Wiggins et al., 2010; Kasinski and Slack, 2012; Cho et al., 2016; Yang et al., 2017). Compared to the control, both nCAR/miR-34a-5p and nCAR/miR-124-3p inhibited cell proliferation to a significantly greater degree (Fig. 5A), which was also demonstrated by the estimated EC50 and Hill Slope values (Supplemental Table 5). Interestingly, H1299 cells (mutant p53) were more sensitive to nCAR/miR-34a-5p than A549 (wild type p53), under which the p53-miR-34a positive feedback loop confers an additional tumor suppressive effect when p53 is haploinsufficient (Okada et al., 2014). Similarly, H1650 and H1975 (mutant EGFR) cells carrying constitutively active EGFR were more sensitive to nCAR/miR-124-3p than A549 (wild type EGFR). In addition, the suppression of A549 cell proliferation was associated with reduced protein levels of miR-34a targets (cMET and CDK6) and miR-124 targets (STAT3, pSTAT3 and MRP4/ABCC4) (Fig. 5B), supporting the presence of multiple targets/pathways for these miRNAs in reducing cancer cell proliferation.

Bioengineered nCAR/miR-34a-5p significantly reduces metastatic lung xenograft tumor growth *in vivo.* Lastly we determined the effectiveness of BERA miR-34a-5p and miR-124-3p

JPET Fast Forward. Published on March 30, 2018 as DOI: 10.1124/jpet.118.247775
This article has not been copyedited and formatted. The final version may differ from this version.

in the suppression of lung tumor progression *in vivo*. Metastatic lung xenograft mouse models were established via tail vein injection of luciferase/GFP-expressing A549 cells and then treated intravenously with *in vivo*-jetPEI-formulated nCAR/miR-34a-5p, nCAR/miR-124-3p, or control RNA (30 μg, three times per week for three weeks). BERAs appeared to be well tolerated in mice because, in addition to normal behaviors, all mice showed a steady increase in body weights that did not differ between treatments (Supplemental Fig. 6A). Tumor growth was monitored over the course of 6 weeks by bioluminescent imaging; and control mice showed stronger signals compared to mice treated with nCAR/miR-34a-5p and nCAR/miR-124-3p (Fig. 6A). At the end of the study, whole lung tissues were excised, weighed, and imaged *ex vivo* (Fig. 6B). As expected, tumors were obvious by visual inspection of lungs collected from mice that showed strong bioluminescent signals, which were indicated by more apparent *ex vivo* GFP signals. Lung tissues from mice treated with nCAR/miR-34a-5p were also found to be significantly lighter than the control group (Supplemental Fig. 6B). Furthermore, we performed histopathological analyses of all excised lung tissues to verify xenograft tumors and quantitatively determine the effectiveness of BERA therapy (Fig. 6C). In agreement with the observations from live animal and *ex vivo* lung images, we found that mice treated with nCAR/miR-34a-5p had significantly lower degrees of lung tumor nodules. These results demonstrate the effectiveness of biologic miR-34a-5p in the control of lung cancer progression in metastatic xenograft mouse models.

Bioengineered have minimal impact on cytokine release in immunocompetent mice *in vivo.* Lastly, we assessed possible immunogenicity of biologic ncRNAs in immunocompetent BALB/c mouse models by measuring the most sensitive cytokines IL-6 and TNFα around the peak time point (1 h after treatment). Our data showed that LPS induced an immediate cytokine release syndrome in mice, as manifested by sharp increase in blood IL-6 and TNFα levels

(Supplemental Fig. 6C). In contrast, compared to untreated mice, administration of *in vivo*-jetPEI-formulated nCAR/miR-34a-5p, nCAR/miR-124-3p, and control RNA just led to insignificant increase of serum IL-6 TNFα levels that are remarkably and significantly lower than LPS treatment. The results indicate that biologic ncRNAs are tolerable in mice with minimal effects on cytokine release.

JPET Fast Forward. Published on March 30, 2018 as DOI: 10.1124/jpet.118.247775
This article has not been copyedited and formatted. The final version may differ from this version.

DISCUSSION

We established a novel ncRNA bioengineering technology following the identification of a stable pre-miR-34a G138U/139ΔG derivative fused to tRNA molecule as a versatile carrier. This platform included the development of new complementary small- and large-scale purification methods. This approach offered a remarkable high-yield (40-80% of total RNAs) and large-scale (4-20 mg from 1 L bacterial fermentation) production of target ncRNAs in *E. coli*, with a high success rate (80%; 33 ncRNAs out of 42). Using two bioengineered ncRNAs as examples, we further demonstrated a selective release of target miRNAs from nCAR/miRNAs and thus specific regulation of target genes, leading to altered miRNome and transcriptome profiles in human cells. In addition, we showed that the introduction of tumor suppressive miR-34a-5p and miR-124-3p with corresponding nCAR/miRNA prodrugs was proven to be effective for the control of human lung cancer cell proliferation *in vitro* and metastatic xenograft tumor progression *in vivo*. These results support the robustness of this new ncRNA bioengineering pipeline and broad applications of biologic ncRNA agents to basic research and experimental therapy.

In sharp contrast to the studies on protein functions and therapeutics using recombinant proteins produced and folded within live cells rather than those made by peptide synthesis, current research on ncRNA macromolecules rely heavily on chemically synthesized ncRNA mimics containing extensive artificial modifications. Although chemical modifications may increase ncRNA stability and thus offer more favorable pharmacokinetic properties (e.g., longer half-life) and even higher potency, synthetic ncRNA agents are fundamentally different molecules that undoubtedly have distinct higher order structures as well as altered chemical and biological properties. Therefore, the relevance of chemo-engineered ncRNAs to cellular ncRNAs needs reconsideration. In addition, synthetic ncRNA agents from different manufacturers vary

largely in the type, site and degree of artificial modifications, which create another layer of uncertainty. Conversely, ncRNAs produced by the bioengineering platform presented in this report resemble the biogenesis of natural ncRNAs in live cells and thus offer highly structured, stable macromolecules without or just with necessary posttranscriptional modifications (Li et al., 2015; Wang et al., 2015). Since recombinant ncRNAs are produced in live cells to tolerable levels, biologic ncRNAs unlikely trigger any severe immune response (Wang et al., 2015; Zhao et al., 2016). Most importantly, the present approach displays substantial advantages over existing recombinant RNA methods (Ponchon and Dardel, 2007; Ponchon et al., 2009; Huang et al., 2013; Chen et al., 2015) because it achieves a remarkable high-level expression of target ncRNA molecules (40-80% of total RNAs) at a high success rate (80%). The resultant ncRNA molecules are also different from viral or non-viral vector/plasmid based ncRNA expression materials that are truly DNA reagents (Ho and Yu, 2016). Therefore, the nCAR-based technology represents a more practical and cost-effective endeavor that can be easily adapted by a general biomedical research lab for the production of ncRNA agents of interest, either in microgram or milligram quantities.

Besides the confirmation of a selective release of target miRNAs from bioengineered nCAR/miRNA agents in human cells, our small RNA sequencing results show that intracellular miRNAs are present as various isoforms, consistent with other studies (Ebhardt et al., 2009; Llorens et al., 2013). This may affect the binding affinity of miRNAs to Ago proteins (Elkayam et al., 2012) or turnover in the cell (Chatterjee and Grosshans, 2009). In particular, nCAR/miR-34a-5p was predominately processed into mature miR-34a-5p as a 22-nt isoform, while other species (21- and 23-nt, shifts in cleavage start site) were produced at much lower abundance. However, nCAR/miR-124-3p was predominantly processed to a 23-nt form in 293T cells, whereas the other 22-nt specie shifted one nt to the right in Dicer-KO cells, whose levels were rather comparable levels. The lack of significant increase of other miRNAs also supports the

selectivity in producing target miRNAs from nCAR/miRNAs, while the proportional decrease of some high-abundance miRNAs could be a result of sharp increase of miR-34a-5p. Moreover, the dependence (miR-34a-5p) and independence (miR-124-3p) on Dicer for processing the nCAR/miRNAs indicate the versatility of using nCAR/miRNAs to introduce particular miRNAs into human cells to selectively change intracellular miRNome. Although it is unknown whether genetic background in Dicer-KO cells remains unchanged or not, our RNA sequencing results support the presence of Dicer-independent factors and pathways for miRNA biogenesis that might be altered in Dicer-KO cells and/or induced by nCAR/miR-124-3p treatment.

Upon the introduction of target miRNA into human cells, bioengineered ncRNA was effective to modulate target gene expression, leading to a specific change of transcriptome profile. Particularly, nCAR/miR-34a-5p and nCAR/miR-124-3p downregulated many well-documented targets (Chang et al., 2007; Karginov et al., 2007; Chi et al., 2009; Kaller et al., 2011) in 293T cells, as well as others (BAG2 and BCL6B for miR-34a; NID1 and VIM for miR-124) not reported before, although synthetic miRNA reagents were not included for comparison in present study. Although those genes have not been experimentally identified or verified by others, many are tentative targets (e.g., BCL6B for miR-34a-5p; and NID1 and VIM for miR-124-3p) predicted by various algorisms such as miRanda (www.microrna.org), TargetScan (http://www.targetscan.org/) and miRWalk (http://zmf.umm.uni-heidelberg.de/apps/zmf/mirwalk/micrornapredictedtarget.html). Some genes (e.g., BAG2) are not predicted targets, whose changes could be consequent or spatially-controlled effects of the changes of primary target gene expression while we cannot rule out possible off-target effects. Nevertheless, the specificity of nCAR/miRNA in the modulation of target gene expression is further demonstrated by “unbiased” enrichment analyses, which identified specific miRNAs behind corresponding downregulated genes. A step towards understanding ncRNAs as biologic

macromolecules may advance our knowledge of these regulators in their natural forms to enable the progression of new discoveries.

As the altered transcriptomes were redefined for multiple intercalating pathways underlying cell growth, proliferation and survival, the antiproliferative activities of nCAR-carried miR-34a-5p and miR-124-3p were observed in multiple human lung carcinoma cell lines. Cells with mutant p53 or constitutively active EGFR backgrounds seem to be more sensitive to miRNA treatment. Since naked biologic RNAs are degradable by serum RNases, formulation is necessary for therapeutic applications (Wang et al., 2015; Jilek et al., 2017). Further studies with in vivo-jetPEI-formulated RNAs in metastatic lung xenograft mouse models not only support the effectiveness of bioengineered miRNA agents *in vivo* but also establish the feasibility of developing biologic ncRNAs as therapeutics. While the sample size was relatively small and nCAR/miR-124-3p treatment group was more variable, the suppression of xenograft tumor growth by nCAR/miR-34a-5p was identified statistically significant than control treatment. Moreover, we demonstrate that biologic ncRNAs are well tolerated in immunocompetent mice, as indicated by minimal impact on cytokine release. Rather, the assessment of biologic ncRNAs for cancer therapy should be challenged by more comprehensive studies with larger sample sizes and different models.

Limited by the array of possible directions, downstream in depth studies were carried out for two of many bioengineered ncRNAs to exemplify their biologic and pharmacological actions in the present study, but warrants additional investigations for bioengineered siRNA and RNA aptamer agents. While we focused on establishing the robust ncRNA bioengineering platform and assessing miRNA replacement strategy (Bader et al., 2010; Rupaimoole and Slack, 2017) with biologic miR-34a-5p and miR-124-3p molecules for lung cancer therapy, the utilities of BERAs cannot be underestimated. As supported by current studies, ncRNA bioengineering technology

and the resulting biologic ncRNA agents should have direct impact on basic biomedical research and development of ncRNA therapies, although current ncRNA carriers may not be extended for the production of long ncRNAs playing important roles in various diseases (Cech and Steitz, 2014; Liu et al., 2017) since longer RNAs are more susceptible for degradation by bacterial RNases (Li et al., 2014; Li et al., 2015).

In summary, we established a novel ncRNA bioengineering technology that can be easily adapted for the production of ncRNA agents bearing sRNAs of interest. Our findings indicate that bioengineered ncRNAs represent unique biologic materials and can be an invaluable addition to current tools for broad biomedical research including the development of ncRNA therapeutics. While we cannot exclude the possibility that more superior ncRNA carriers would be expanded, the principle of producing biologic ncRNA macromolecules for basic and translational research will remain. We speculate the capability of multiplexing biologic ncRNAs in the near future for identification of new ncRNA actions and potential therapeutics.

AUTHOR CONTRIBUTIONS

Participated in research design: Yu and Ho.

Conducted experiments: Ho, Duan, Batra, Jilek, Tu, and Qiu.

Contributed new reagents or analytic tools: Yu, Qiu, Hu, Wun, Lara, DeVere White, and Chen.

Performed data analysis: Ho, Yu, Duan, Qiu, and Hu.

Wrote or contributed to the writing of the manuscript: Ho, Yu, Qiu and Hu.

REFERENCES

An, J., J. Lai, M. L. Lehman and C. C. Nelson (2013). miRDeep*: an integrated application tool for miRNA identification from RNA sequencing data. *Nucleic Acids Res* **41**: 727-737.

Bader, A. G., D. Brown and M. Winkler (2010). The promise of microRNA replacement therapy. *Cancer Res* **70**: 7027-7030.

Beckert, B. and B. Masquida (2011). Synthesis of RNA by in vitro transcription. *Methods Mol Biol* **703**: 29-41.

Beg, M. S., A. J. Brenner, J. Sachdev, M. Borad, Y. K. Kang, J. Stoudemire, S. Smith, A. G. Bader, S. Kim and D. S. Hong (2017). Phase I study of MRX34, a liposomal miR-34a mimic, administered twice weekly in patients with advanced solid tumors. *Invest New Drugs* **35**: 180-188.

Bogerd, H. P., A. W. Whisnant, E. M. Kennedy, O. Flores and B. R. Cullen (2014). Derivation and characterization of Dicer- and microRNA-deficient human cells. *RNA* **20**: 923-937.

Bramsen, J. B. and J. Kjems (2012). Development of Therapeutic-Grade Small Interfering RNAs by Chemical Engineering. *Front Genet* **3**: 154.

Butash, K. A., P. Natarajan, A. Young and D. K. Fox (2000). Reexamination of the effect of endotoxin on cell proliferation and transfection efficiency. *Biotechniques* **29**: 610-614, 616, 618-619.

Cech, T. R. and J. A. Steitz (2014). The noncoding RNA revolution-trashing old rules to forge new ones. *Cell* **157**: 77-94.

Chang, T. C., E. A. Wentzel, O. A. Kent, K. Ramachandran, M. Mullendore, K. H. Lee, G. Feldmann, M. Yamakuchi, M. Ferlito, C. J. Lowenstein, D. E. Arking, M. A. Beer, A. Maitra and J. T. Mendell (2007). Transactivation of miR-34a by p53 broadly influences gene expression and promotes apoptosis. *Mol Cell* **26**: 745-752.

Chatterjee, S. and H. Grosshans (2009). Active turnover modulates mature microRNA activity in Caenorhabditis elegans. *Nature* **461**: 546-549.

Chen, Q. X., W. P. Wang, S. Zeng, S. Urayama and A. M. Yu (2015). A general approach to high-yield biosynthesis of chimeric RNAs bearing various types of functional small RNAs for broad applications. *Nucleic Acids Res* **43**: 3857-3869.

Chi, S. W., J. B. Zang, A. Mele and R. B. Darnell (2009). Argonaute HITS-CLIP decodes microRNA-mRNA interaction maps. *Nature* **460**: 479-486.

Cho, C. Y., J. S. Huang, S. G. Shiah, S. Y. Chung, J. D. Lay, Y. Y. Yang, G. M. Lai, A. L. Cheng, L. T. Chen and S. E. Chuang (2016). Negative feedback regulation of AXL by miR-34a modulates apoptosis in lung cancer cells. *RNA* **22**: 303-315.

Corey, D. R. (2007). Chemical modification: the key to clinical application of RNA interference? *J Clin Invest* **117**: 3615-3622.

Ebhardt, H. A., H. H. Tsang, D. C. Dai, Y. Liu, B. Bostan and R. P. Fahlman (2009). Meta-analysis of small RNA-sequencing errors reveals ubiquitous post-transcriptional RNA modifications. *Nucleic Acids Res* **37**: 2461-2470.

Elkayam, E., C. D. Kuhn, A. Tocilj, A. D. Haase, E. M. Greene, G. J. Hannon and L. Joshua-Tor (2012). The structure of human argonaute-2 in complex with miR-20a. *Cell* **150**: 100-110.

Fang, P. Y., L. M. Gomez Ramos, S. Y. Holguin, C. Hsiao, J. C. Bowman, H. W. Yang and L. D. Williams (2017). Functional RNAs: combined assembly and packaging in VLPs. *Nucleic Acids Res* **45**: 3519-3527.

Hatziapostolou, M., C. Polytarchou, E. Aggelidou, A. Drakaki, G. A. Poultsides, S. A. Jaeger, H. Ogata, M. Karin, K. Struhl, M. Hadzopoulou-Cladaras and D. Iliopoulos (2011). An HNF4alpha-miRNA inflammatory feedback circuit regulates hepatocellular oncogenesis. *Cell* **147**: 1233-1247.

Ho, P. Y. and A. M. Yu (2016). Bioengineering of noncoding RNAs for research agents and therapeutics. *Wiley Interdiscip Rev RNA* **7**: 186-197.

Hornung, V., M. Guenthner-Biller, C. Bourquin, A. Ablasser, M. Schlee, S. Uematsu, A. Noronha, M. Manoharan, S. Akira, A. de Fougerolles, S. Endres and G. Hartmann (2005). Sequence-specific potent induction of IFN-alpha by short interfering RNA in plasmacytoid dendritic cells through TLR7. *Nat Med* **11**: 263-270.

Huang, L., J. Jin, P. Deighan, E. Kiner, L. McReynolds and J. Lieberman (2013). Efficient and specific gene knockdown by small interfering RNAs produced in bacteria. *Nat Biotechnol* **31**: 350-356.

Jilek, J. L., Y. Tian and A. M. Yu (2017). Effects of MicroRNA-34a on the Pharmacokinetics of Cytochrome P450 Probe Drugs in Mice. *Drug Metab Dispos* **45**: 512-522.

Kaller, M., S. T. Liffers, S. Oeljeklaus, K. Kuhlmann, S. Roh, R. Hoffmann, B. Warscheid and H. Hermeking (2011). Genome-wide characterization of miR-34a induced changes in protein and mRNA expression by a combined pulsed SILAC and microarray analysis. *Mol Cell Proteomics* **10**: M111 010462.

Karginov, F. V., C. Conaco, Z. Xuan, B. H. Schmidt, J. S. Parker, G. Mandel and G. J. Hannon (2007). A biochemical approach to identifying microRNA targets. *Proc Natl Acad Sci U S A* **104**: 19291-19296.

Kasinski, A. L. and F. J. Slack (2012). miRNA-34 prevents cancer initiation and progression in a therapeutically resistant K-ras and p53-induced mouse model of lung adenocarcinoma. *Cancer Res* **72**: 5576-5587.

Khvorova, A. and J. K. Watts (2017). The chemical evolution of oligonucleotide therapies of clinical utility. *Nat Biotechnol* **35**: 238-248.

Lewis, B. P., C. B. Burge and D. P. Bartel (2005). Conserved seed pairing, often flanked by adenosines, indicates that thousands of human genes are microRNA targets. *Cell* **120**: 15-20.

Li, B. and C. N. Dewey (2011). RSEM: accurate transcript quantification from RNA-Seq data with or without a reference genome. *BMC Bioinformatics* **12**: 323.

Li, H. and R. Durbin (2009). Fast and accurate short read alignment with Burrows-Wheeler transform. *Bioinformatics* **25**: 1754-1760.

Li, M. M., B. Addepalli, M. J. Tu, Q. X. Chen, W. P. Wang, P. A. Limbach, J. M. LaSalle, S. Zeng, M. Huang and A. M. Yu (2015). Chimeric MicroRNA-1291 Biosynthesized Efficiently in Escherichia coli Is Effective to Reduce Target Gene Expression in Human Carcinoma Cells and Improve Chemosensitivity. *Drug Metab Dispos* **43**: 1129-1136.

Li, M. M., W. P. Wang, W. J. Wu, M. Huang and A. M. Yu (2014). Rapid Production of Novel Pre-MicroRNA Agent hsa-mir-27b in Escherichia coli Using Recombinant RNA Technology for Functional Studies in Mammalian Cells. *Drug Metab Dispos* **42**: 1791-1795.

Li, P. C., M. J. Tu, P. Y. Ho, J. L. Jilek, Z. Duan, Q. Y. Zhang, A. X. Yu and A. M. Yu (2018). Bioengineered NRF2-siRNA Is Effective to Interfere with NRF2 Pathways and Improve Chemosensitivity of Human Cancer Cells. *Drug Metab Dispos* **46**: 2-10.

Liu, C., Z. Yang, J. Wu, L. Zhang, S. Lee, D. J. Shin, M. Tran and L. Wang (2017). lncRNA H19 interacts with polypyrimidine tract-binding protein 1 to reprogram hepatic lipid homeostasis. *Hepatology*.

Llorens, F., M. Hummel, L. Pantano, X. Pastor, A. Vivancos, E. Castillo, H. Mattlin, A. Ferrer, M. Ingham, M. Noguera, R. Kofler, J. C. Dohm, R. Pluvinet, M. Bayes, H. Himmelbauer, J. Antonio del Rio, E. Marti and L. Sumoy (2013). Microarray and deep sequencing cross-platform analysis of the mirRNome and isomiR variation in response to epidermal growth factor. *BMC Genomics* **14**.

Malyala, P. and M. Singh (2008). Endotoxin limits in formulations for preclinical research. *J Pharm Sci* **97**: 2041-2044.

Markova, S. M. and D. L. Kroetz (2014). ABCC4 is regulated by microRNA-124a and microRNA-506. *Biochem Pharmacol* **87**: 515-522.

Okada, N., C. P. Lin, M. C. Ribeiro, A. Biton, G. Lai, X. He, P. Bu, H. Vogel, D. M. Jablons, A. C. Keller, J. E. Wilkinson, B. He, T. P. Speed and L. He (2014). A positive feedback between p53 and miR-34 miRNAs mediates tumor suppression. *Genes Dev* **28**: 438-450.

Park, J. E., I. Heo, Y. Tian, D. K. Simanshu, H. Chang, D. Jee, D. J. Patel and V. N. Kim (2011). Dicer recognizes the 5' end of RNA for efficient and accurate processing. *Nature* **475**: 201-205.

Pereira, P., A. Q. Pedro, J. A. Queiroz, A. R. Figueiras and F. Sousa (2017). New insights for therapeutic recombinant human miRNAs heterologous production: Rhodovolum sulfidophilum vs Escherichia coli. *Bioengineered*: 1-8.

Pereira, P. A., J. F. Tomas, J. A. Queiroz, A. R. Figueiras and F. Sousa (2016). Recombinant pre-miR-29b for Alzheimer s disease therapeutics. *Sci Rep* **6**: 19946.

Ponchon, L., G. Beauvais, S. Nonin-Lecomte and F. Dardel (2009). A generic protocol for the expression and purification of recombinant RNA in Escherichia coli using a tRNA scaffold. *Nat Protoc* **4**: 947-959.

Ponchon, L. and F. Dardel (2007). Recombinant RNA technology: the tRNA scaffold. *Nat Methods* **4**: 571-576.

Robbins, M., A. Judge and I. MacLachlan (2009). siRNA and innate immunity. *Oligonucleotides* **19**: 89-102.

Robinson, M. D., D. J. McCarthy and G. K. Smyth (2010). edgeR: a Bioconductor package for differential expression analysis of digital gene expression data. *Bioinformatics* **26**: 139-140.

Rupaimoole, R. and F. J. Slack (2017). MicroRNA therapeutics: towards a new era for the management of cancer and other diseases. *Nat Rev Drug Discov* **16**: 203-222.

Siegel, R. L., K. D. Miller and A. Jemal (2017). Cancer Statistics, 2017. *CA Cancer J Clin* **67**: 7-30.

Sun, F., H. Fu, Q. Liu, Y. Tie, J. Zhu, R. Xing, Z. Sun and X. Zheng (2008). Downregulation of CCND1 and CDK6 by miR-34a induces cell cycle arrest. *FEBS Lett* **582**: 1564-1568.

Thyagarajan, A., A. Shaban and R. P. Sahu (2018). MicroRNA-Directed Cancer Therapies: Implications in Melanoma Intervention. *J Pharmacol Exp Ther* **364**: 1-12.

Wang, W. P., P. Y. Ho, Q. X. Chen, B. Addepalli, P. A. Limbach, M. M. Li, W. J. Wu, J. L. Jilek, J. X. Qiu, H. J. Zhang, T. Li, T. Wun, R. D. White, K. S. Lam and A. M. Yu (2015). Bioengineering Novel Chimeric microRNA-34a for Prodrug Cancer Therapy: High-Yield Expression and Purification, and Structural and Functional Characterization. *J Pharmacol Exp Ther* **354**: 131-141.

Wiggins, J. F., L. Ruffino, K. Kelnar, M. Omotola, L. Patrawala, D. Brown and A. G. Bader (2010). Development of a lung cancer therapeutic based on the tumor suppressor microRNA-34. *Cancer Res* **70**: 5923-5930.

Yamakuchi, M., M. Ferlito and C. J. Lowenstein (2008). miR-34a repression of SIRT1 regulates apoptosis. *Proc Natl Acad Sci U S A* **105**: 13421-13426.

Yang, Q., L. Wan, C. Xiao, H. Hu, L. Wang, J. Zhao, Z. Lei and H. T. Zhang (2017). Inhibition of LHX2 by miR-124 suppresses cellular migration and invasion in non-small cell lung cancer. *Oncol Lett* **14**: 3429-3436.

Zhao, Y., M. J. Tu, W. P. Wang, J. X. Qiu, A. X. Yu and A. M. Yu (2016). Genetically engineered pre-microRNA-34a prodrug suppresses orthotopic osteosarcoma xenograft tumor growth via the induction of apoptosis and cell cycle arrest. *Sci Rep* **6**: 26611.

Footnotes

This work was supported in part by the National Institutes of Health [Grants R01GM113888 and U01CA175315 (A.M.Y.); P30CA093373 (R.D.V.W. and P.N.L.)]. J.L.J. was supported by a NIGMS-funded Pharmacology Training Program grant [T32GM099608]. The authors also thank Drs. Qiu-Xia Chen and Junjian Wang for their technical supports and helpful discussion.

Send reprint requests to: Prof. Ai-Ming Yu, Department of Biochemistry & Molecular Medicine, UC Davis School of Medicine, Sacramento, CA 95817, USA; Email: aimyu@ucdavis.edu.

JPET Fast Forward. Published on March 30, 2018 as DOI: 10.1124/jpet.118.247775
This article has not been copyedited and formatted. The final version may differ from this version.

Figure Legends

FIGURE 1. Identification of a new ncRNA carrier (nCAR) towards higher-level expression of recombinant RNAs. (*A*) tRNA standalone showed no expression in HST08 *E. coli*, whereas (*B*) the fusion of a Sephadex aptamer (highlighted in orange) led to an overexpression of resulting MSA. (*C*) Hybrid MSA/mir-34a was overexpressed in *E. coli* and pre-miR-34a itself showed relatively lower-level expression. (*D*) The pre-miR-34a was refined toward a more stable structure (base changes dictated by red arrows), and the Sephadex aptamer was removed. Among these constructs, the tRNA/pre-miR-34a-G138U/139ΔG showed the highest level of heterogeneous expression (~50% of total RNAs) and therefore, was chosen as a carrier for ncRNA bioengineering.

FIGURE 2. Three-step strategy to bioengineer ncRNA agents using nCAR. (*A*) In step 1, the ncRNAs of interest are cloned into the target vector (Supplementary Fig. S2), where the miR-34a duplex (red/green) is replaced by target sRNAs (e.g., miRNA, siRNA or antisense RNA, RNA aptamers, etc.) of interest. (*B*) In step 2, the verified plasmid is transformed into *E. coli*, and total RNAs are isolated post-fermentation for urea-PAGE analysis of target BERA expression. Among 42 target ncRNAs, 33 showed remarkable high-level expression (40-80% of total RNAs). Total RNAs from untransformed wild-type bacteria (WT) are used for comparison. (*C*) Lastly in step 3, ncRNAs are isolated either on small scale using spin columns or large scale using fast protein liquid chromatography (FPLC) methods to offer micrograms or milligrams of BERAs, respectively. B, blank nontransformed *E. coli*; T, total RNA; FT, flow-through; W1-2, washes; E, eluate. Fractions 1-11 were collected at various times during FPLC isolation. RNA purity was verified by high performance liquid chromatography (HPLC) analysis (Supplementary Fig. S3), and both methods could offer >98% pure, ready-to-use BERAs.

JPET Fast Forward. Published on March 30, 2018 as DOI: 10.1124/jpet.118.247775
This article has not been copyedited and formatted. The final version may differ from this version.

FIGURE 3. Selective release of target miRNAs from nCAR/miRNAs in human cells, in a Dicer dependent (miR-34a) and independent (miR-124) manner, changes miRNome profiles. (*A*) Small RNA sequencing analyses showed that (i) nCAR/miR-34a-5p and nCAR/miR-124-3p were selectively processed to target miR-34a-5p and miR-124-3p isoforms (length, starting site/position), respectively, in human cells (fold of change (FC), nCAR/miR versus control tRNA (con) treatment); and (ii) the level of miR-34a-5p (reads or rds) produced from BERA was largely affected by Dicer status, whereas miR-124-3p production was Dicer independent. Individual read counts represent enriched miRNAs with FC > 1.2 or < 0.8 with differential significance by EdgeR analysis. (*B*) miR-34a-5p became the most abundant miRNA in both wild type and Dicer-KO cells after transfection with nCAR-miR-34a-5p, which was in sharp contrast to a nominal portion in control cells. Similarly, miR-124-3p became the seventh-most and most abundant miRNA in wild type and Dicer-KO cells, respectively, after transfection with nCAR-miR-124-3p.

FIGURE 4. Specificity of nCAR/miRNA in the regulation of miRNA target gene expression. (*A*) Volcano plots of significantly-altered mRNAs ($P < 0.01$) in 293T cells transfected with nCAR/miR-34a-5p or miR-124-3p, as compared to control. Many transcripts were downregulated in 293T cells by nCAR/miR. In Dicer-KO cells, nCAR/miR-34a-5p showed minimal impact on the transcriptome (only 6 genes were significantly downregulated), while effects of nCAR/miR-124-3p retained. Several reported targets of miR-34a-5p (blue) and miR-124-3p (red) are designated with arrows. (*B*) Heatmap of the top 30 most downregulated genes in wild type and Dicer-KO 293T cells treated with nCAR/miRNA, as compared to the control tRNA treatment. (*C*) Specificity of BERA in the regulation of miRNA target genes is supported by miRNA enrichment analyses, which readily identified miR-34/449 underlying nCAR/miR-34a-5p-downregulated mRNAs in 293T cells, whereas not in Dicer-KO cells. By contrast, miR-124/506 was enriched for nCAR/miR-124-3p-downregulated mRNAs in both wild type and

Dicer-KO 293T cells, which supports not only the specificity of BERA/miR-124-3p in the modulation of target gene expression but also its independence on Dicer. (*D*) Gene regulatory networks of major biological pathways affected by miR-34a-5p and miR-124-3p, respectively, as identified by Ingenuity Pathway Analysis (IPA).

FIGURE 5. Bioengineered miR-34a and miR-124 inhibit human lung cancer cell proliferation via the suppression of (proto-)oncogene expression. (*A*) Dose-response curves of nCAR/miR-34a-5p and nCAR-miR-124-3p in inhibiting human lung carcinoma A549, H23, H1299, H1650, and H1975 cell proliferation. Each nCAR/miR is significantly more effective than control RNA ($P < 0.001$, two-way ANOVA with Bonferroni post-tests), except miR-34a-5p against H1975 cells. Values are mean ± SD (N = 3 per group). (*B*) Estimated EC50 and Hill Slope values. Data were fit to the normalized dose response relationship with variable slope. Values are mean ± SD (N = 3 per group). *$P < 0.05$, **$P < 0.01$, and ***$P < 0.001$, compared to corresponding control (1-way ANOVA). (*C*) Antiproliferative effects were associated with downregulation of miRNA target gene expression (cMET and CDK6 for miR-34a; STAT3, pSTAT3 and ABCC4/MRP4 for miR-124), as demonstrated by Western blots. *$P < 0.05$, Student's t-test.

FIGURE 6. Application of bioengineered miRNAs to control lung xenograft tumor progression *in vivo*. (*A*) Effects of nCAR/miR-34a-5p, nCAR/miR-124-3p and control RNA treatment on the progression of lung tumor progression in metastatic xenograft tumor mouse models (N = 9 per group), which were monitored through live animal bioluminescent imaging after the administration of D-luciferin. Bioluminescent images were taken on days 10, 20, 25, 32, 39 post inoculation of A549 cells and normalized to the same exposure time. (*B*) Local lung xenograft tumors were assessed via GFP imaging of *ex vivo* lung tissues at the end of the

JPET Fast Forward. Published on March 30, 2018 as DOI: 10.1124/jpet.118.247775
This article has not been copyedited and formatted. The final version may differ from this version.

study. (*C*) Representative H&E-stained slides of lung tumors (100×). The tumor areas were thus quantified as percentages of corresponding lung areas, which were significantly ($P < 0.05$) lower for nCAR/miR-34a-5p treatment than the control.

JPET Fast Forward. Published on March 30, 2018 as DOI: 10.1124/jpet.118.247775
This article has not been copyedited and formatted. The final version may differ from this version.

Table 1. Yields and purities of individual BERAs produced on a large scale using the nCAR platform and isolated by FPLC method.

nCAR	Yield (mg RNA/L fermentation)	Purity (%; by HPLC)
miR-27a-3p	10.1	99.4
miR-27b-3p	10.2	99.4
miR-451a-5p	18.8	98.9
ApoB-siRNA	17.0	99.0
anti-miR-126-3p	20.0	99.2
ICAM1-siRNA	12.0	98.6
miR-298-5p	15.4	97.2
miR-519c-5p	16.0	99.3
miR-122-5p	9.80	87.0
Nrf2-siRNA	18.7	98.3
miR-126-3p	11.6	99.8
miR-144-5p	10.6	98.7
ARV7-siRNA	17.0	99.3
GFP-siRNA	12.0	99.3
let-7c-5p	8.70	92.4
miR-127-3p	3.83	95.5
miR-34a-5p	16.6	98.3
miR-124-3p	8.34	98.3
miR-328-3p	14.8	99.7
anti-miR-451b-5p	11.3	99.3
MSA	5.72	99.6
anti-miR-21-5p-3	7.48	98.2
miR-33a-5p	7.54	96.0
anti-miR-21-5p-2	9.41	96.9
anti-miR-122-5p	7.67	99.3
scrm-5	7.54	53.5
scrm-4	7.43	98.2
scrm-3	8.54	99.3
anti-miR-21-5p	11.7	99.4
miR-34a/TPA3'+TPA5'	18.2	99.5
miR-888/pegaptanib3'	16.0	98.3
miR-34a/EpCAMA3'	12.7	99.0

Figure 1

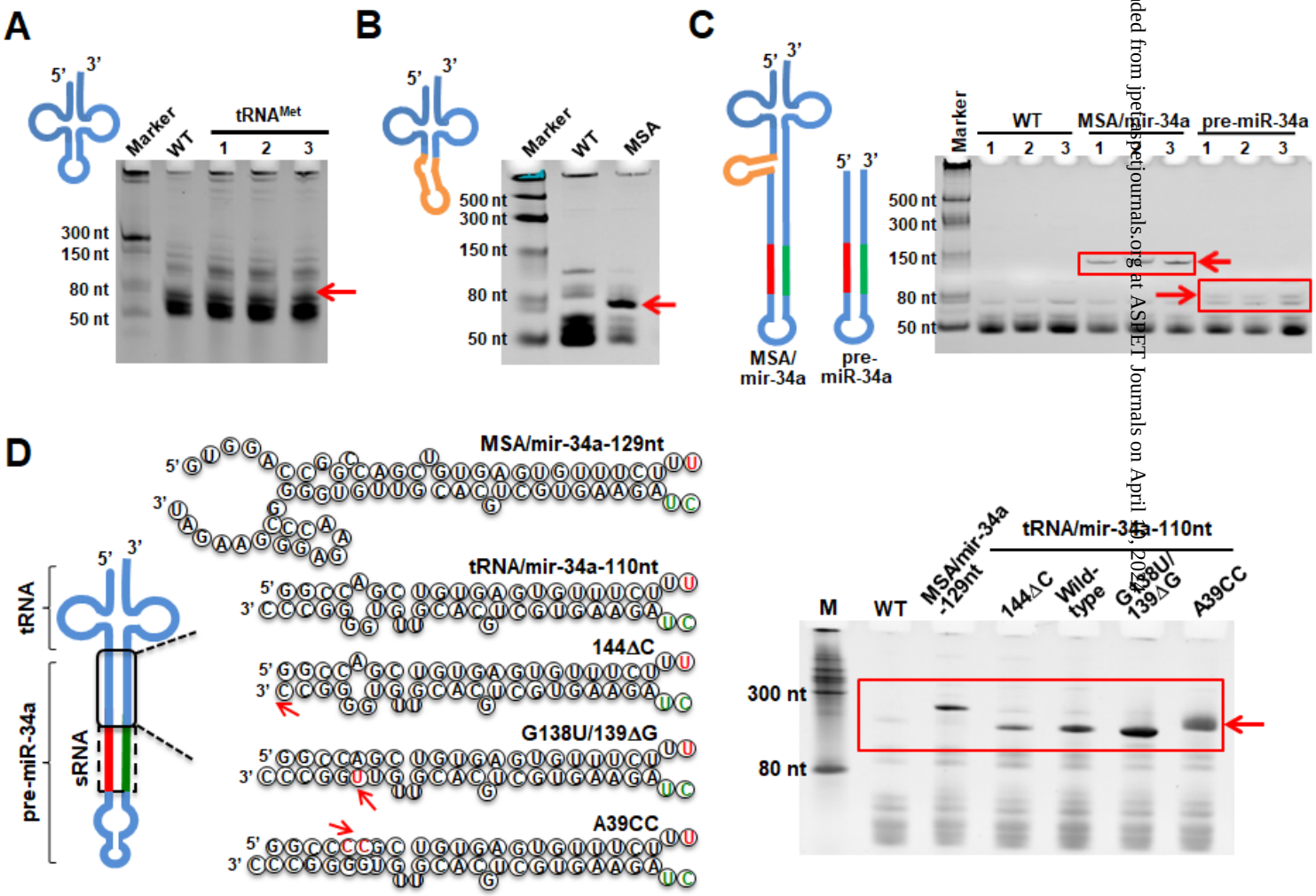

Figure 2

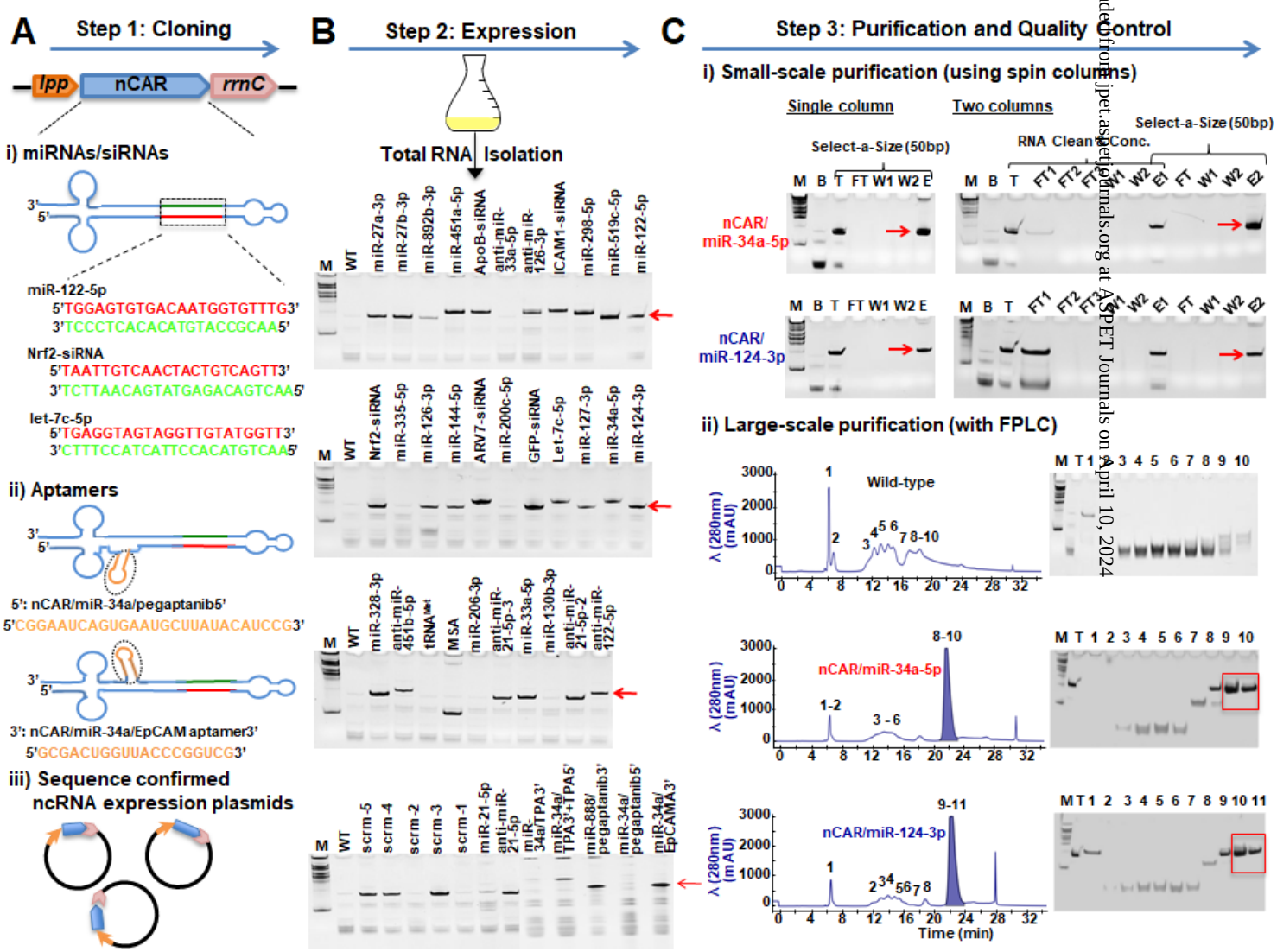

Figure 3

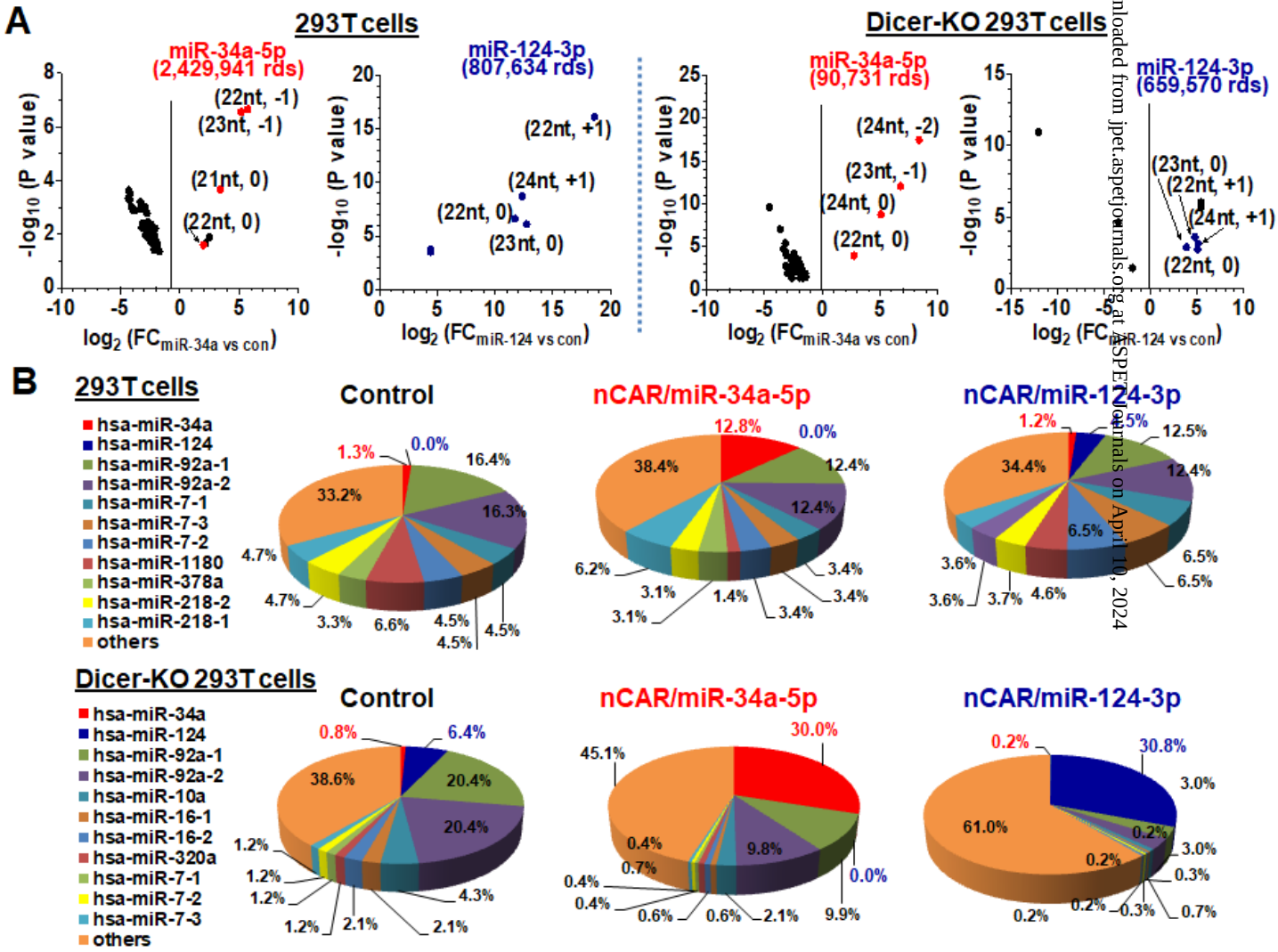

Figure 4

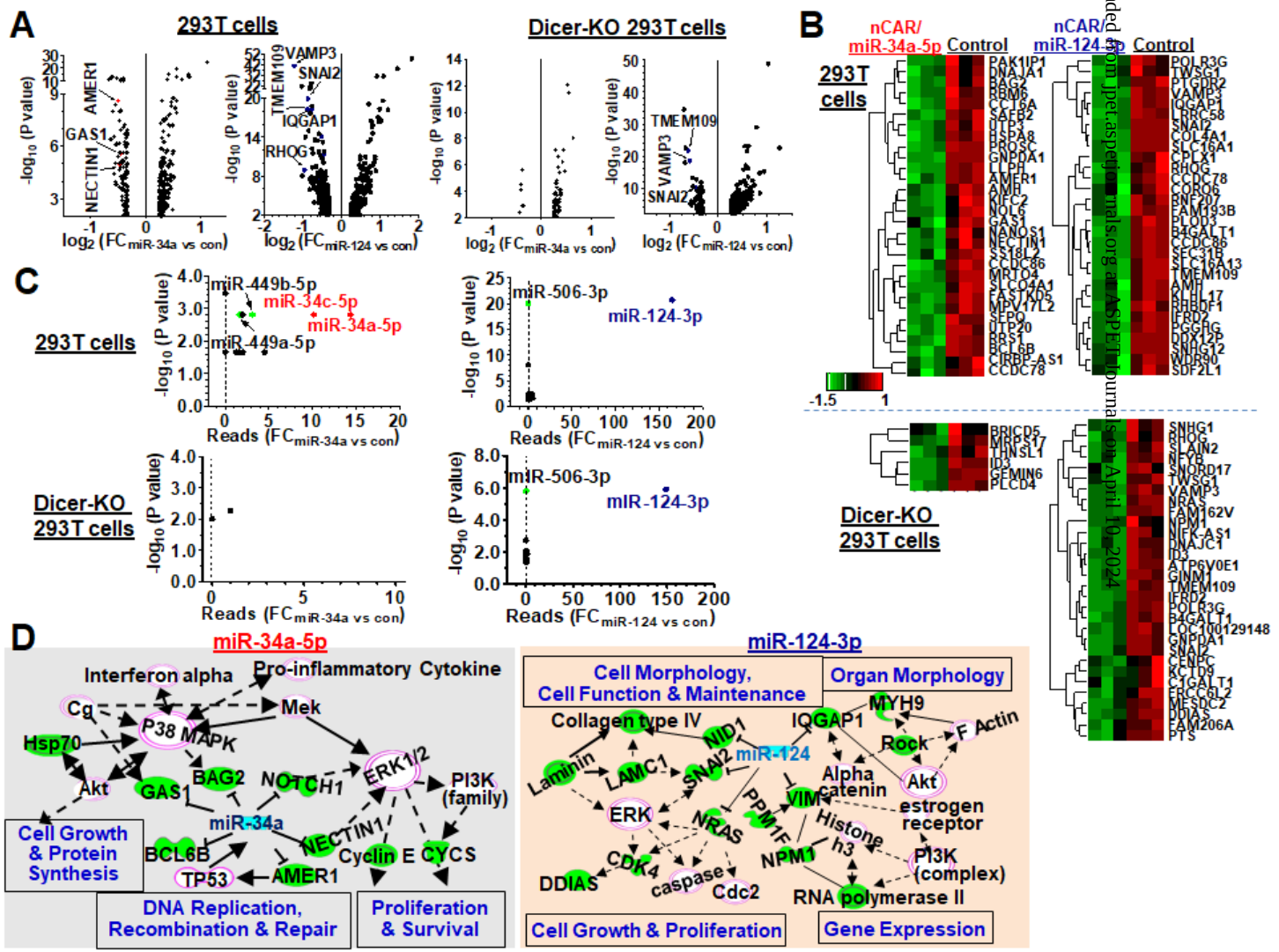

Figure 5

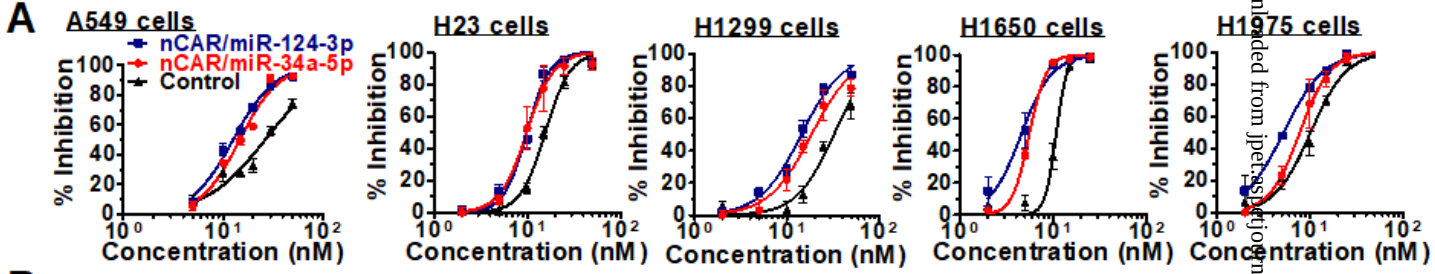

B

Cell line	Control		nCAR/miR-34a-5p		nCAR/miR-124-3p	
	EC50 (nM)	Hill slope	EC50 (nM)	Hill slope	EC50 (nM)	Hill slope
A549	26.5 ± 1.06	1.46 ± 0.14	14.8 ± 1.04***	2.24 ± 0.19**	12.6 ± 1.03***	2.09 ± 0.13*
H23	15.7 ± 1.03	3.27 ± 0.26	9.93 ± 1.05***	3.02 ± 0.43	9.96 ± 1.03***	3.55 ± 0.39
H1299	32.5 ± 1.05	2.12 ± 0.21	18.6 ± 1.06***	1.87 ± 0.19	14.4 ± 1.04***	1.93 ± 0.14
H1650	10.8 ± 1.02	7.42 ± 1.43	5.54 ± 1.01**	4.79 ± 0.30	4.54 ± 1.06***	2.63 ± 0.33***
H1975	10.2 ± 1.06	2.25 ± 0.29	7.80 ± 1.04	2.67 ± 0.23	5.22 ± 1.02**	2.00 ± 0.07

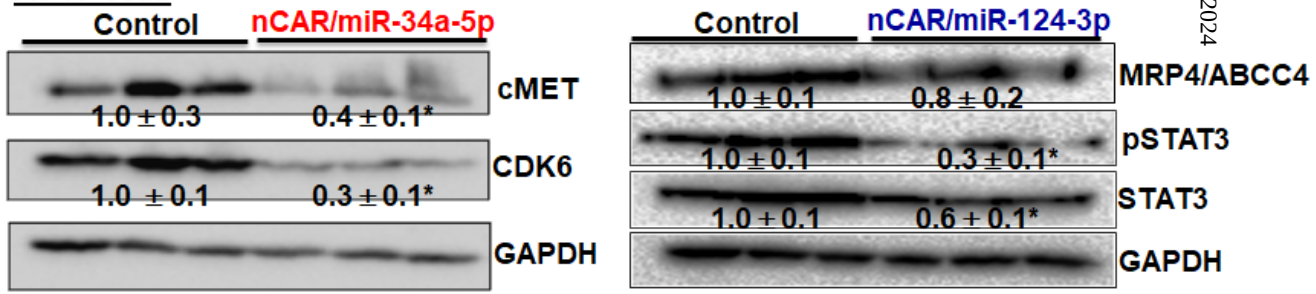

Figure 6

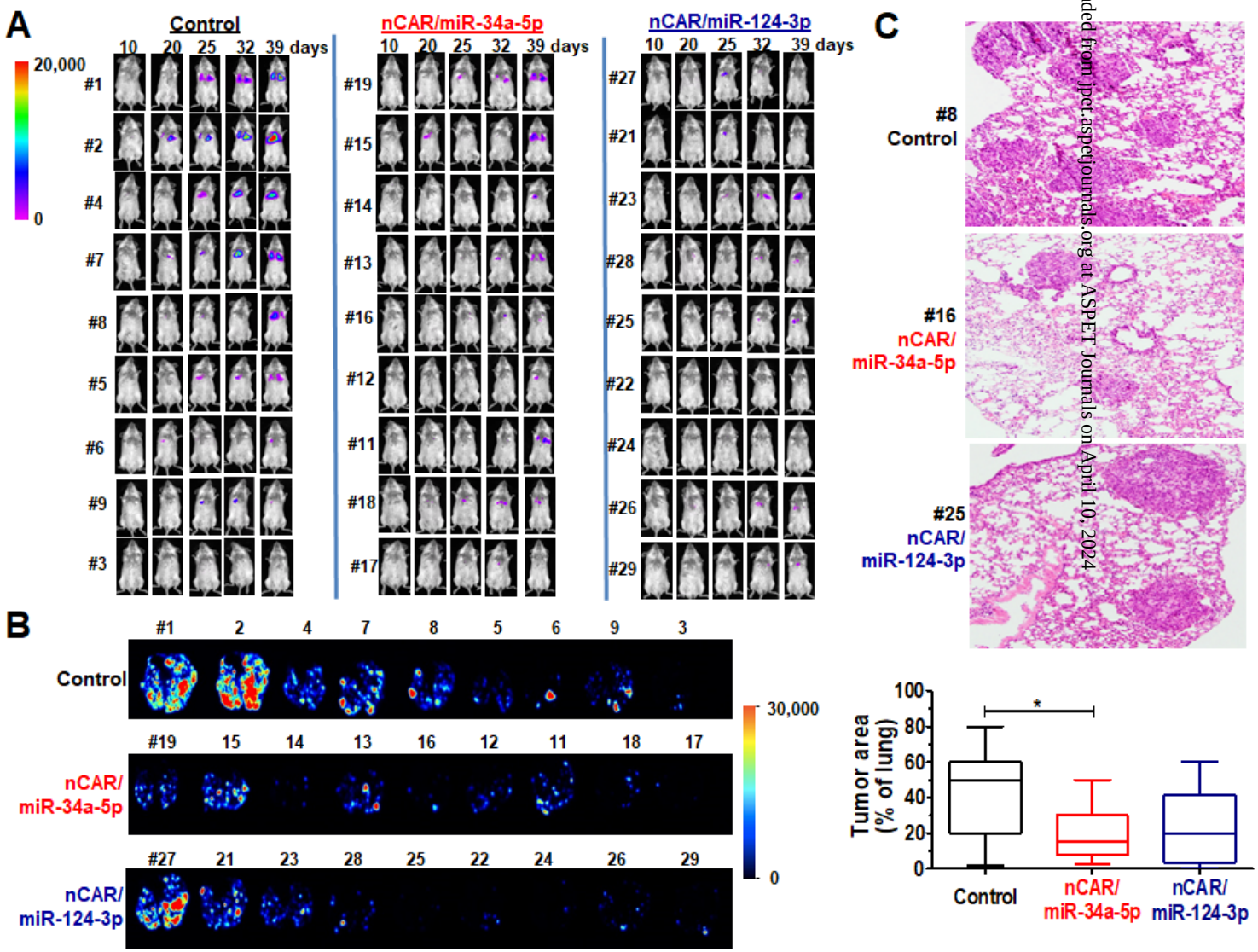

Bioengineered ncRNAs selectively change cellular miRNome profiles for cancer therapy

Pui Yan Ho, Zhijian Duan, Neelu Batra, Joseph L. Jilek, Mei-Juan Tu, Jing-Xin Qiu, Zihua Hu, Theodore Wun, Primo N. Lara, Ralph W. DeVere White, Hongwu Chen, Ai-Ming Yu*

Supplementary Materials

Supplemental Figures 1 to 7

Supplemental Tables 1 to 4

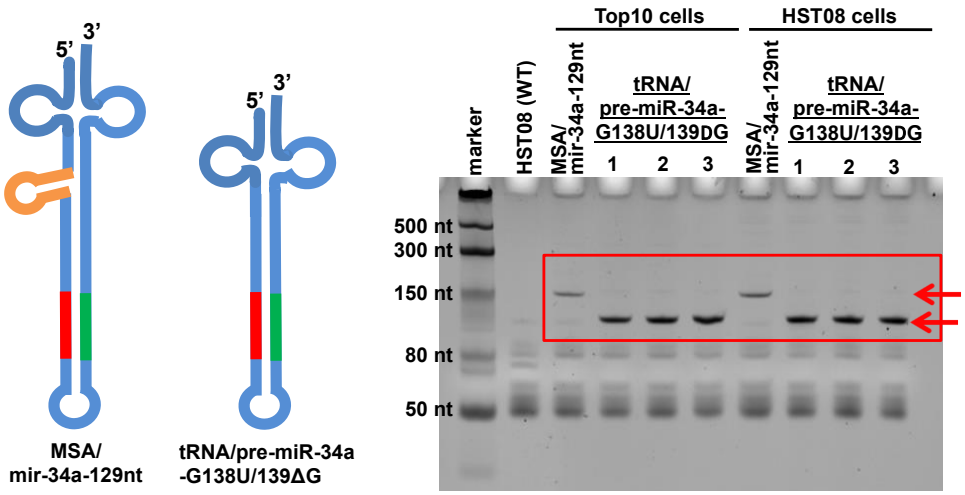

Supplemental Figure 1. Independence on Sephadex aptamer for heterogeneous expression of ncRNAs in *E. coli*. The refined pre-miR-34a G138U/139ΔG fused to standalone tRNA is expressed at higher level than MSA/mir-34a-129nt in both HST08 and Top10 cells. Total RNAs were analysed by urea-PAGE.

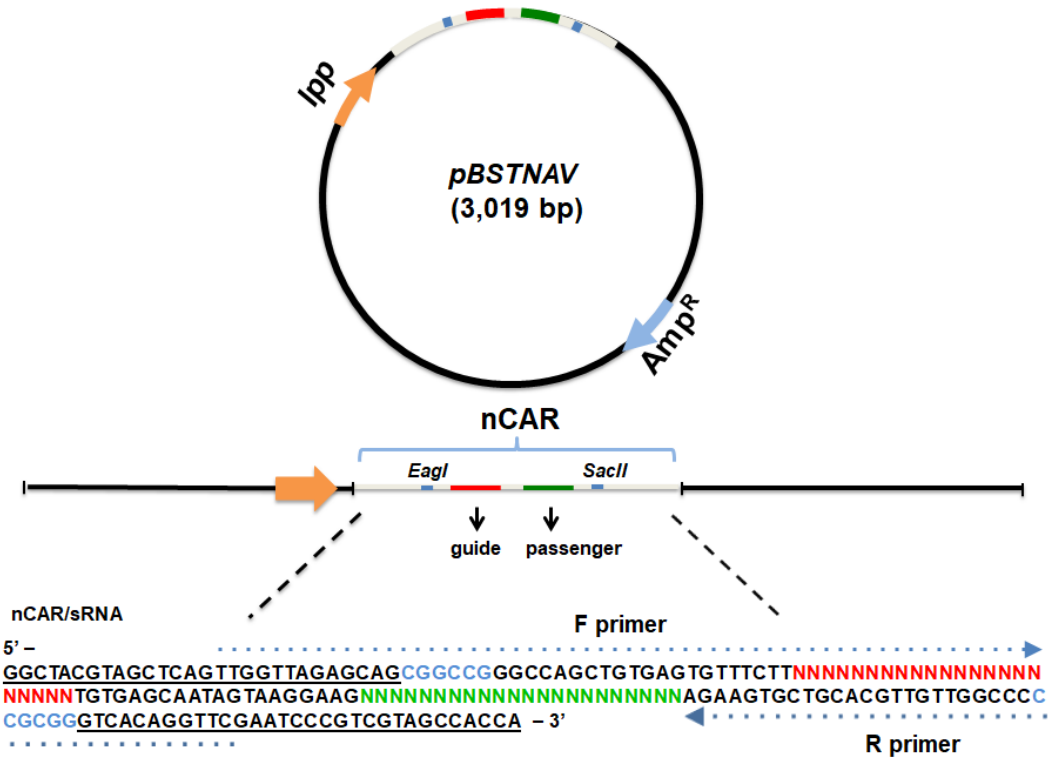

Supplemental Figure 2. Map of nCAR-based plasmid for the production of BERAs. nCAR was placed into the pBSTNAV vector, driven under *lpp* promoter and selected via ampicillin resistance (*Amp*^{R}). The mature miRNA and complementary sequences (highlighted in red and green, respectively) within nCAR may be substituted by a miRNA/siRNA of interest. Cloning primers are thus designed to span the 15-nt from restriction site (blue), partially overlapping pre-miR-34a spanning towards the target ncRNA on both ends.

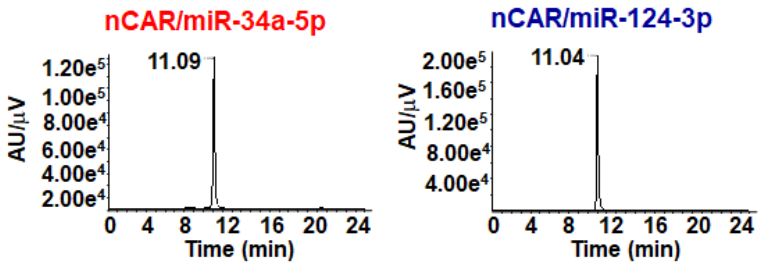

Supplemental Figure 3. HPLC determination of the purity of isolated BERAs. Shown are the HPLC traces of nCAR/miR-34a-5p and nCAR/miR-124-3p purified by anion exchange FPLC on a large scale, which are both over 98% pure.

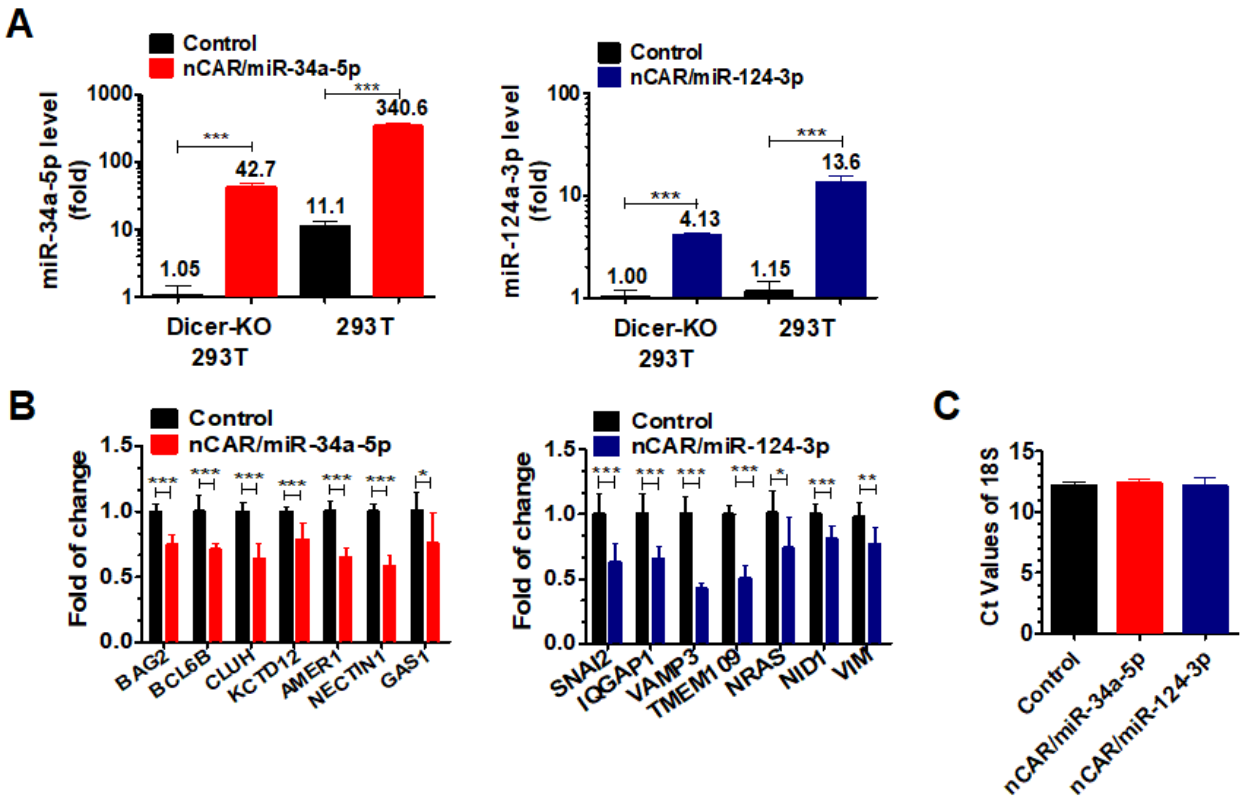

Supplemental Figure 4. qPCR verification of the degree of changes in target miRNAs and some mRNAs identified by RNA sequencing study. (*A*) Stem-loop RT qPCR quantification confirmed the degree of change in miR-34a-5p and miR-124-3p levels in wild type and Dicer-KO cells after treated with BERAs. Values are mean ± SD (N = 3 per group). ***P < 0.001; unpaired t-test. **(***B*) RT-qPCR validation of some downregulated transcripts in 293T cells identified by RNA sequencing study. AMER1, NECTIN1, and GAS1 are targets reported previously for miR-34a-5p; and SNAI2, IQGAP1, VAMP3, TMEM109, and NRAS are known targets for miR-124-3p. Values are mean ± SD (N = 9 per group). ***P < 0.001; two-way ANOVA with Bonferroni post-tests. (*C*) Ct values of 18S housekeeping gene were not altered by nCAR/miRNA treatments.

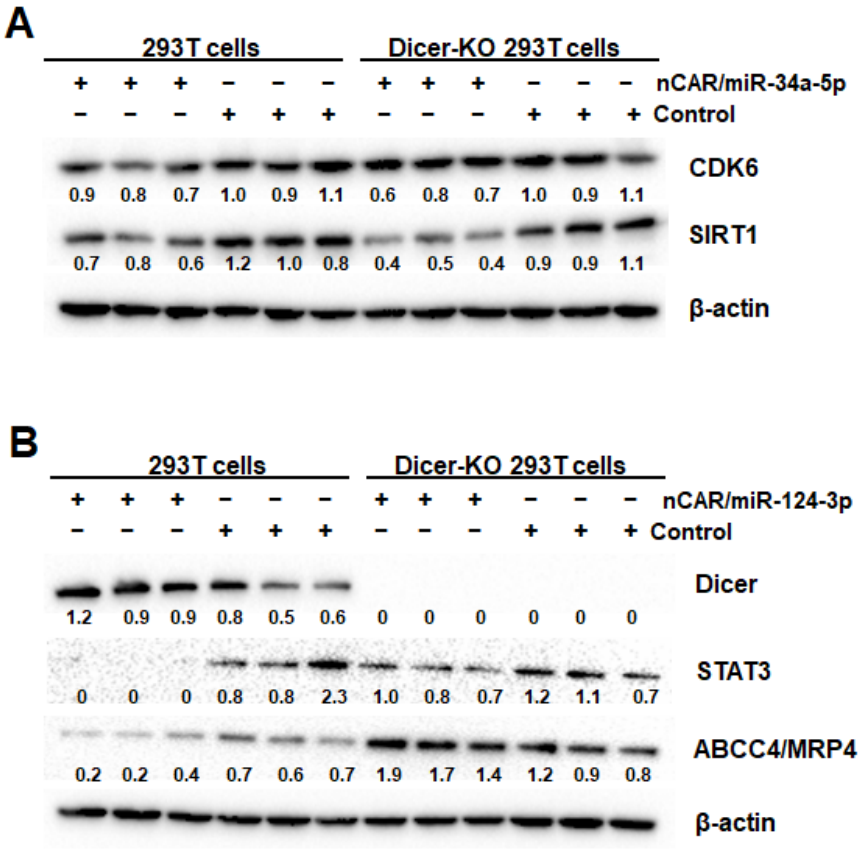

Supplemental Figure 5. Impact of Dicer status on the control of protein levels of target genes by bioengineered miR-34a and miR-124. (*A*) High levels of miR-34a-5p produced from nCAR/miR-34a-5p led to a consistent reduction of protein levels of miR-34a targets (e.g., CDK6 and SIRT1) in 293T cells, whereas the effects might disappear (CDK6) or retain (SIRT1) in Dicer-KO cells due a much lower level of miR-34a-5p. (*B*) The production of miR-124-3p at distinct lengths and positions in wild-type and Dicer-KO cells could cause different effects on the protein expression of some known miR-124 targets (e.g., STAT3 and MRP4). Western blots were conducted with selected antibodies, and β-actin was used as a loading control.

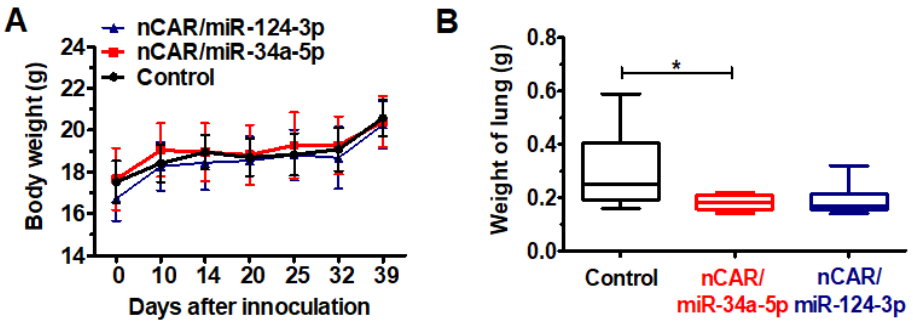

Supplemental Figure 6. (*A*) Mouse body weights showed a steady increase during the treatments and did not differ between treatment groups ($P > 0.05$; two-way ANOVA), suggesting that BERA therapeutics were well tolerated in mice. (*B*) Weights of the xenograft lungs were significantly lower for nCAR/miR-34a-5p treatment, as compared to the control (*$P < 0.05$; one-way ANOVA with Dunnett's Multiple Comparison Test), suggesting the control of metastatic lung xenograft tumor progression. Values are mean ± SD (N = 9 per group).

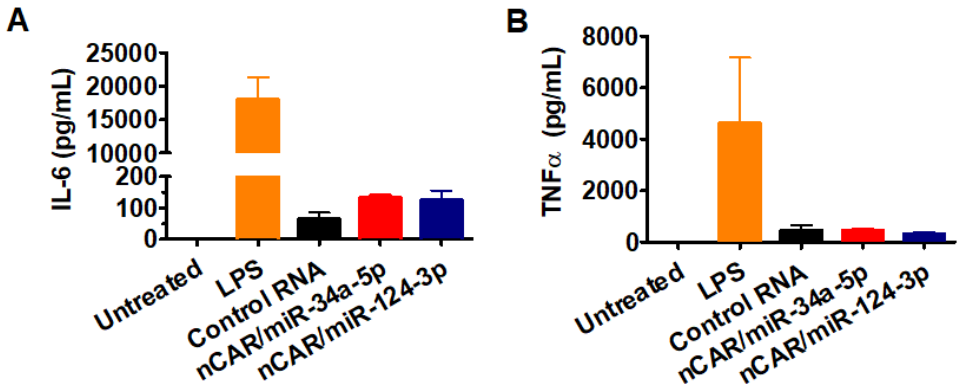

Supplemental Figure 7. Bioengineered RNAs have minor effects on cytokine release in immunocompetent BALB/c mice, as indicated by minimal changes of serum IL-6 (*A*) and TNFα (*B*) levels. Untreated mice and mice treated with lipopolysaccharide (LPS) were used as controls, and cytokine levels were determined by ELISA. IL-6 and TNFα levels in LPS-treated mice are significantly ($P < 0.01$; 1-way ANOVA) higher than all other groups, whereas none of the RNA treatment group is statistically different from untreated mice. Values are mean ± SD (N = 4 mice per group).

Supplemental Table 1. List of siRNA and RNA aptamer sequences obtained from literature for bioengineering of target ncRNA agents.

Name	RNA Sequence (5' – 3')	Reference
Apolipoprotein B-siRNA (ApoB-siRNA)	GCCUCAGUCUGCUUCGCACC	(Raal et al., 2010)
ICAM1-siRNA	GCCCAAGCUGGCAUCCGUCA	(Miner et al., 2004)
Nrf2-siRNA	UAAUUGUCAACUUCUGUCA	(Feinstein, 2013)
ARV7-siRNA	GUAGUUGUAAGUAUCAUGA	(Liu et al., 2014)
GFP-siRNA	AGUUGUACUCCAGCUUGUGCCC	(Chen et al., 2015)
Theophylline Aptamer (TPA)	GGCGAUACCAGCCGAAAGGCCCUUGGCAGCGUC	(Zimmermann et al., 2000)
Pegaptanib	CGGAAUCAGUGAAUGCUUAUACAUCCG	(Ng et al., 2006)
EpCAM Aptamer (EpCAMA)	GCGACUGGUUACCCGGUCG	(Shigdar et al., 2011)
scrm-1	GUGUAACACGUCUAUACGCCCA	(Schober et al., 2014)
scrm-2	GUUCGUCUGUAGACGGUUGUUG	http://www.genscript.com/siRNA_target_finder.html
scrm-3	UUCUCCGAAGCUGUCACGUUU	(Luan et al., 2010)
scrm-4	AAGCGCGCUUUGUAGGAUUCGU	(Nakatsu et al., 2013)
scrm-5	GGUGUCGUUUCUCUGGUGAGUA	http://www.invivogen.com/sirnawizard/

Supplemental Table 2. Sequences of target BERAs and primers used for the construction of corresponding plasmids. Underlined are tRNA sequences; target miRNA/siRNA sequences are highlighted in red and complementary sequences are in green; aptamer sequences are highlighted in orange.

Pre-miR-34a derivatives

Name	# nts	RNA Sequence	MW (Da)	Primers (5' - 3') to clone corresponding coding sequence	
MSA/ mir-34a-129nt	233	GGCUACGUAGCUCAGUUGGUUAGAGCAGCGGCCGAGUAAUUUACGUCGACGUGGACCGGCCAGCUGUGAGUGUUUCUUUGGCAGUGUCUUAGCUGGUUGUUGUGAGCAAUAGUAAGGAAGCAAUCAGCAAGUAUACUGCCCUAGAAGUGCUGCACGUUGUGGGGCCCAAGAGGGAAGAUGACGUCGAUGGUUGCGGCCGCGGGUCACAGGUUCGAAUCCCGUCGUAGCCACCA	75,604	F	AGTAATTTACGTCGACGTGGACCGGCCAGCTGTGAGTGTT
				R	CGGCCGCAACCATCGACGTCATCTTCCCTCTTGGGCCCCACAACG
tRNA/ mir-34a-110nt 144ΔC	180	GGCUACGUAGCUCAGUUGGUUAGAGCAGCGGCCGGGCCAGCUGUGAGUGUUUCUUUGGCAGUGUCUUAGCUGGUUGUUGUGAGCAAUAGUAAGGAAGCAAUCAGCAAGUAUACUGCCCUAGAAGUGCUGCACGUUGUGGGGCCCCGCGGGUCACAGGUUCGAAUCCCGUCGUAGCCACCA	58,322	F	GTTAGAGCAGCGGCCGGGCCAGCTGTGAGTGTTTCTTTG
				R	TCGAACCTGTGACCCGCGGGGCCCCACAACGTGCAG
tRNA/ mir-34a-110nt Wild type	181	GGCUACGUAGCUCAGUUGGUUAGAGCAGCGGCCGGGCCAGCUGUGAGUGUUUCUUUGGCAGUGUCUUAGCUGGUUGUUGUGAGCAAUAGUAAGGAAGCAAUCAGCAAGUAUACUGCCCUAGAAGUGCUGCACGUUGUGGGGCCCCCGCGGGUCACAGGUUCGAAUCCCGUCGUAGCCACCA	58,627	F	GTTAGAGCAGCGGCCGGGCCAGCTGTGAGTGTTTCTTTG
				R	TCGAACCTGTGACCCGCGGGGGCCCCACAACGTGCAG
tRNA/ mir-34a-110nt G138U/ 139ΔG	180	GGCUACGUAGCUCAGUUGGUUAGAGCAGCGGCCGGGCCAGCUGUGAGUGUUUCUUUGGCAGUGUCUUAGCUGGUUGUUGUGAGCAAUAGUAAGGAAGCAAUCAGCAAGUAUACUGCCCUAGAAGUGCUGCACGUUGUUGGCCCCCGCGGGUCACAGGUUCGAAUCCCGUCGUAGCCACCA	58,243	F	GTTAGAGCAGCGGCCGGGCCAGCTGTGAGTGTTTCTTTG
				R	TCGAACCTGTGACCCGCGGGGGCCAACAACGTGCAGC
tRNA/ mir-34a-110nt A39CC	182	GGCUACGUAGCUCAGUUGGUUAGAGCAGCGGCCGGGCCCCGCUGUGAGUGUUUCUUUGGCAGUGUCUUAGCUGGUUGUUGUGAGCAAUAGUAAGGAAGCAAUCAGCAAGUAUACUGCCCUAGAAGUGCUGCACGUUGUGGGGCCCCCGCGGGUCACAGGUUCGAAUCCCGUCGUAGCCACCA	58,908	F	GTTAGAGCAGCGGCCGGGCCCCGCTGTGAGTGTTTC
				R	TCGAACCTGTGACCCGCGGGGGCCCCACAACGTGCAG

nCAR/sRNAs

Name	# nts	RNA Sequence	MW (Da)	Primers (5' - 3')	
miR-	181	GGCUACGUAGCUCAGUUGGUUAGAGCAGCGGCCGGGCCAGCUG	58,580	F	GTTAGAGCAGCGGCCGGGCCAGCTGTGAGTGTT

27a-3p		UGAGUGUUUCUUUUCACAGUGGCUAAGUUCCGCUUGUGAGCAAU AGUAAGGAAGGCAGGGCUUAGCUGCUUGUGACUAGAAGUGCUGC ACGUUGUUGGCCCCCGCGGGUCACAGGUUCGAAUCCCGUCGUAG CCACCA		F	TCTTTTCACAGTGGCTAAGTTCCGCTTGTGAGCA ATAGTAA
				R	TCGAACCTGTGACCCGCGGGGGCCAACAACGTG CAGCACTTCTAGTCACAAGCAGCTAAGCCCTGCC TTCCTTACTATTGC
miR-27b-3p	180	GGCUACGUAGCUCAGUUGGUUAGAGCAGCGGCCGGGCCAGCUG UGAGUGUUUCUUUUCACAGUGGCUAAGUUCUGCUUGUGAGCAAU AGUAAGGAAGGCAGAGCUAGCUCAUUGUGACCAGAAGUGCUGCA CGUUGUUGGCCCCCGCGGGUCACAGGUUCGAAUCCCGUCGUAGC CACCA	58,242	F	GTTAGAGCAGCGGCCGGGCCAGCTGTGAGTGTT TCTTTTCACAGTGGCTAAGTTCTGCTTGTGAGCAA TAGTAA
				R	TCGAACCTGTGACCCGCGGGGGCCAACAACGTG CAGCACTTCTGGTCACAGTGAGCTAGCTCTGCCT TCCTTACTATTGC
miR-892b-3p	180	GGCUACGUAGCUCAGUUGGUUAGAGCAGCGGCCGGGCCAGCUG UGAGUGUUUCUUCACUGGCUCCUUUCUGGGUAGAUGUGAGCAAU AGUAAGGAAUCUACUCAGAAGUGAGCCAGUUUAGAAGUGCUGCA CGUUGUUGGCCCCCGCGGGUCACAGGUUCGAAUCCCGUCGUAGC CACCA	58,203	F	GTTAGAGCAGCGGCCGGGCCAGCTGTGAGTGTT TCTTCACTGGCTCCTTTCTGGGTAGATGTGAGCA ATAGTAA
				R	TCGAACCTGTGACCCGCGGGGGCCAACAACGTG CAGCACTTCTAAACTGGCTCACTTCTGAGTAGATT CCTTACTATTGC
miR-451a-5p	180	GGCUACGUAGCUCAGUUGGUUAGAGCAGCGGCCGGGCCAGCUG UGAGUGUUUCUUAAACCGUUACCAUUACUGAGUUUGUGAGCAAU AGUAAGGAAGACUUAGUAUGGUUAAUGGUUCUAGAAGUGCUGCA CGUUGUUGGCCCCCGCGGGUCACAGGUUCGAAUCCCGUCGUAGC CACCA	58,198	F	GTTAGAGCAGCGGCCGGGCCAGCTGTGAGTGTT TCTTAAACCGTTACCATTACTGAGTTTGTGAGCAA TAGTAA
				R	TCGAACCTGTGACCCGCGGGGGCCAACAACGTG CAGCACTTCTAGAACCATTAACCATACTAAGTCTT CCTTACTATTGC
ApoB-siRNA	180	GGCUACGUAGCUCAGUUGGUUAGAGCAGCGGCCGGGCCAGCUG UGAGUGUUUCUUUGCCUCAGUCUGCUUCGCACCUUGUGAGCAAU AGUAAGGAAGGGUGCGAACAGUACUGAGGCCUAGAAGUGCUGCA CGUUGUUGGCCCCCGCGGGUCACAGGUUCGAAUCCCGUCGUAGC CACCA	58,232	F	GTTAGAGCAGCGGCCGGGCCAGCTGTGAGTGTT TCTTTGCCTCAGTCTGCTTCGCACCTTGTGAGCA ATAGTAA
				R	TCGAACCTGTGACCCGCGGGGGCCAACAACGTG CAGCACTTCTAGGCCTCAGTACTGTTCGCACCCT TCCTTACTATTGC
anti-miR-33a-5p	180	GGCUACGUAGCUCAGUUGGUUAGAGCAGCGGCCGGGCCAGCUG UGAGUGUUUCUUACCACCAGAACAUGCAAUGCAAUGUGAGCAAUA GUAAGGAAUUGCAUUGCGUAUUCUGGUGGGUAGAAGUGCUGCAC GUUGUUGGCCCCCGCGGGUCACAGGUUCGAAUCCCGUCGUAGCC ACCA	58,273	F	GTTAGAGCAGCGGCCGGGCCAGCTGTGAGTGTT TCTTACCACCAGAACATGCAATGCAATGTGAGCA AT
				R	TCGAACCTGTGACCCGCGGGGGCCAACAACGTG CAGCACTTCTACCCACCAGAATACGCAATGCAAT TCCTTA
anti-miR-126-3p	180	GGCUACGUAGCUCAGUUGGUUAGAGCAGCGGCCGGGCCAGCUG UGAGUGUUUCUUAGCAUGGCACUCAUUAUUACGCUGUGAGCAAU AGUAAGGAAGCGUAAUAAGAGUUGCCAUGCCUAGAAGUGCUGCA CGUUGUUGGCCCCCGCGGGUCACAGGUUCGAAUCCCGUCGUAGC CACCA	58,233	F	GTTAGAGCAGCGGCCGGGCCAGCTGTGAGTGTT TCTTAGCATGGCACTCATTATTACGCTGTGAGCA ATAGTAA
				R	TCGAACCTGTGACCCGCGGGGGCCAACAACGTG CAGCACTTCTAGGCATGGCAACTCTTATTACGCT TCCTTACTATTGC
ICAM1-siRNA	180	GGCUACGUAGCUCAGUUGGUUAGAGCAGCGGCCGGGCCAGCUG UGAGUGUUUCUUUGCCCAAGCUGGCAUCCGUCAUUGUGAGCAAU	58,232	F	GTTAGAGCAGCGGCCGGGCCAGCTGTGAGTGTT TCTTTGCCCAAGCTGGCATCCGTCATTGTGAGCA

		AGUAAGGAAGUGACGGAUCCAUGCUUGGGCCUAGAAGUGCUGCA CGUUGUUGGCCCCCGCGGGUCACAGGUUCGAAUCCCGUCGUAGC CACCA			ATAGTAA
				R	TCGAACCTGTGACCCGCGGGGGCCAACAACGTG CAGCACTTCTAGGCCCAAGCATGGATCCGTCACT TCCTTACTATTGC
miR-298-5p	180	GGCUACGUAGCUCAGUUGGUUAGAGCAGCGGCCGGGCCAGCUG UGAGUGUUUCUUAGCAGAAGCAGGGAGGUUCUCCCAUGAGCAAU AGUAAGGAGGGGAGAACCCCCAUGCUUUUGACAGAAGUGCUGCA CGUUGUUGGCCCCCGCGGGUCACAGGUUCGAAUCCCGUCGUAGC CACCA	58,364	F	GTTAGAGCAGCGGCCGGGCCAGCTGTGAGTGTT TCTTAGCAGAAGCAGGGAGGTTCTCCCATGAGCA ATAGTAA
				R	TCGAACCTGTGACCCGCGGGGGCCAACAACGTG CAGCACTTCTGTCAAAAGCATGGGGGTTCTCCCC TCCTTACTATTGC
miR-519c-5p	180	GGCUACGUAGCUCAGUUGGUUAGAGCAGCGGCCGGGCCAGCUG UGAGUGUUUCUUCUCUAGAGGGAAGCGCUUUCUGUGUGAGCAAU AGUAAGGAACAGAAAGUGCAUCUUUUUAGAUUAGAAGUGCUGCAC GUUGUUGGCCCCCGCGGGUCACAGGUUCGAAUCCCGUCGUAGCC ACCA	58,252	F	GTTAGAGCAGCGGCCGGGCCAGCTGTGAGTGTT TCTTCTCTAGAGGGAAGCGCTTTCTGTGTGAGCA ATAGTAA
				R	TCGAACCTGTGACCCGCGGGGGCCAACAACGTG CAGCACTTCTAATCTAAAAAGATGCACTTTCTGTT CCTTACTATTGC
miR-122-5p	180	GGCUACGUAGCUCAGUUGGUUAGAGCAGCGGCCGGGCCAGCUG UGAGUGUUUCUUUGGAGUGUGACAAUGGUGUUUGUGUGAGCAAU AGUAAGGAACAAACGCCAUGUACACACUCCCUAGAAGUGCUGCAC GUUGUUGGCCCCCGCGGGUCACAGGUUCGAAUCCCGUCGUAGCC ACCA	58,249	F	GTTAGAGCAGCGGCCGGGCCAGCTGTGAGTGTT TCTTTGGAGTGTGACAATGGTGTTTGTGTGAGCA ATAGTAA
				R	TCGAACCTGTGACCCGCGGGGGCCAACAACGTG CAGCACTTCTAGGGAGTGTGTACATGGCGTTTGT TCCTTACTATT
Nrf2-siRNA	180	GGCUACGUAGCUCAGUUGGUUAGAGCAGCGGCCGGGCCAGCUG UGAGUGUUUCUUUAAUUGUCAACUACUGUCAGUUUGUGAGCAAU AGUAAGGAAAACUGACAGAGUAUGACAAUUCUAGAAGUGCUGCAC GUUGUUGGCCCCCGCGGGUCACAGGUUCGAAUCCCGUCGUAGCC ACCA	58,188	F	GTTAGAGCAGCGGCCGGGCCAGCTGTGAGTGTT TCTTTAATTGTCAACTACTGTCAGTTTGTGAGCAA TAGTA
				R	TCGAACCTGTGACCCGCGGGGGCCAACAACGTG CAGCACTTCTAGAATTGTCATACTCTGTCAGTTTT CCTTACTAT
miR-335-5p	181	GGCUACGUAGCUCAGUUGGUUAGAGCAGCGGCCGGGCCAGCUG UGAGUGUUUCUUUCAAGAGCAAUAACGAAAAAUGUUGUGAGCAAU AGUAAGGAACCGUUUUUCAUUAUGCUCUUGCUAGAAGUGCUGCA CGUUGUUGGCCCCCGCGGGUCACAGGUUCGAAUCCCGUCGUAGC CACCA	58,470	F	GTTAGAGCAGCGGCCGGGCCAGCTGTGAGTGTT TCTTTCAAGAGCAATAACGAAAAATGTTGTGAGCA A
				R	TCGAACCTGTGACCCGCGGGGGCCAACAACGTG CAGCACTTCTAGCAAGAGCATAATGAAAAACGGT TCCTTAC
miR-126-3p	180	GGCUACGUAGCUCAGUUGGUUAGAGCAGCGGCCGGGCCAGCUG UGAGUGUUUCUUUCGUACCGUGAGUAAUAAUGCGUGUGAGCAAU AGUAAGGAAGUGCAUUAUUCUCUAUGGUACGCAGAAGUGCUGCA CGUUGUUGGCCCCCGCGGGUCACAGGUUCGAAUCCCGUCGUAGC CACCA	58,228	F	GTTAGAGCAGCGGCCGGGCCAGCTGTGAGTGTT TCTTTCGTACCGTGAGTAATAATGCGTGTGAGCA A
				R	TCGAACCTGTGACCCGCGGGGGCCAACAACGTG CAGCACTTCTGCGTACCATAGAGAATAATGCACT TCCTTACT
miR-144-5p	180	GGCUACGUAGCUCAGUUGGUUAGAGCAGCGGCCGGGCCAGCUG UGAGUGUUUCUUGGAUAUCAUCAUAUACUGUAAGUGUGAGCAAU AGUAAGGAAUUUACAGUAAUGUAUGAUAUCAUAGAAGUGCUGCAC	58,214	F	GTTAGAGCAGCGGCCGGGCCAGCTGTGAGTGTT TCTTGGATATCATCATATACTGTAAGTGTGAGCAA TAGTA

		GUUGUUGGCCCCCGCGGGUCACAGGUUCGAAUCCCGUCGUAGCCACCA		R	TCGAACCTGTGACCCGCGGGGGCCAACAACGTGCAGCACTTCTATGATATCATACATTACTGTAAATTCCTTACTATTG
ARV7-siRNA	180	GGCUACGUAGCUCAGUUGGUUAGAGCAGCGGCCGGGCCAGCUGUGAGUGUUUCUUGUAGUUGUAAGUAUCAUGAUGUUGUGAGCAAUAGUAAGGAAGCAUCAUGAACUAUACAACUAAUAGAAGUGCUGCACGUUGUUGGCCCCCGCGGGUCACAGGUUCGAAUCCCGUCGUAGCCACCA	58,252	F	GTTAGAGCAGCGGCCGGGCCAGCTGTGAGTGTTTCTTGTAGTTGTAAGTATCATGATGTTGTGAGCAATAGTAA
				R	TCGAACCTGTGACCCGCGGGGGCCAACAACGTGCAGCACTTCTATTAGTTGTATAGTTCATGATGCTTCCTTACTATTGC
miR-200c-5p	180	GGCUACGUAGCUCAGUUGGUUAGAGCAGCGGCCGGGCCAGCUGUGAGUGUUUCUUCGUCUUACCCAGCAGUGUUUGGUGUGAGCAAUAGUAAGGAAUCAAACACUCUGUGGUAAGACCUAGAAGUGCUGCACGUUGUUGGCCCCCGCGGGUCACAGGUUCGAAUCCCGUCGUAGCCACCA	58,186	F	GTTAGAGCAGCGGCCGGGCCAGCTGTGAGTGTTTCTTCGTCTTACCCAGCAGTGTTTGGTGTGAGCAATAGTAA
				R	TCGAACCTGTGACCCGCGGGGGCCAACAACGTGCAGCACTTCTAGGTCTTACCACAGAGTGTTTGATTCCTTACTATTG
GFP-siRNA	180	GGCUACGUAGCUCAGUUGGUUAGAGCAGCGGCCGGGCCAGCUGUGAGUGUUUCUUAGUUGUACUCCAGCUUGUGCCCUGUGAGCAAUAGUAAGGAAGGGCACAAGUGGUAGUACAACCUAGAAGUGCUGCACGUUGUUGGCCCCCGCGGGUCACAGGUUCGAAUCCCGUCGUAGCCACCA	58,264	F	GTTAGAGCAGCGGCCGGGCCAGCTGTGAGTGTTTCTTAGTTGTACTCCAGCTTGTGCCCTGTGAGCAATAGTAA
				R	TCGAACCTGTGACCCGCGGGGGCCAACAACGTGCAGCACTTCTAGGTTGTACTACCACTTGTGCCCTTCCTTACTATTGC
let-7c-5p	181	GGCUACGUAGCUCAGUUGGUUAGAGCAGCGGCCGGGCCAGCUGUGAGUGUUUCUUUGAGGUAGUAGGUUGUAUGGUUUGUGAGCAAUAGUAAGGAAGAACUGUACACCUUACUACCUUUCAGAAGUGCUGCACGUUGUUGGCCCCCGCGGGUCACAGGUUCGAAUCCCGUCGUAGCCACCA	58,535	F	GTTAGAGCAGCGGCCGGGCCAGCTGTGAGTGTTTCTTTGAGGTAGTAGGTTGTATGGTTTGTGAGCAA
				R	TCGAACCTGTGACCCGCGGGGGCCAACAACGTGCAGCACTTCTGAAAGGTAGTAAGGTGTACAGTTCTTCCTTACT
miR-127-3p	185	GGCUACGUAGCUCAGUUGGUUAGAGCAGCGGCCGGGCCAGCUGUGAGUGUUUCUAUCGGAUCCGUCUGAGCUUGGCUUGUGAGCAAUAGUAAGGAAAGCCUGCUGAAGCUCAGAGGGCUCUGAUAGAAGUGCUGCACGUUGUUGGCCCCCGCGGGUCACAGGUUCGAAUCCCGUCGUAGCCACCA	59,927	F	GTTAGAGCAGCGGCCGGGCCAGCTGTGAGTGTTTCTATCGGATCCGTCTGAGCTTGGCTTGTGAGCAAT
				R	TCGAACCTGTGACCCGCGGGGGCCAACAACGTGCAGCACTTCTATCAGAGCCCTCTGAGCTTCAGCAGGCTTTCCTTA
miR-34a-5p	180	GGCUACGUAGCUCAGUUGGUUAGAGCAGCGGCCGGGCCAGCUGUGAGUGUUUCUUUGGCAGUGUCUUAGCUGGUUGUUGUGAGCAAUAGUAAGGAAGCAAUCAGCAAGUAUACUGCCCUAGAAGUGCUGCACGUUGUUGGCCCCCGCGGGUCACAGGUUCGAAUCCCGUCGUAGCCACCA	58,243	F	GTTAGAGCAGCGGCCGGGCCAGCTGTGAGTGTTTCTTTG
				R	TCGAACCTGTGACCCGCGGGGGCCAACAACGTGCAGC
miR-124-3p	180	GGCUACGUAGCUCAGUUGGUUAGAGCAGCGGCCGGGCCAGCUGUGAGUGUUUCUUUAAGGCACGCGGUGAAUGCCGUUGUGAGCAAUAGUAAGGAAGCGGUGUUCCCGUCGUGCCUUCUAGAAGUGCUGCACGUUGUUGGCCCCCGCGGGUCACAGGUUCGAAUCCCGUCGUAGCCACCA	58,265	F	GTTAGAGCAGCGGCCGGGCCAGCTGTGAGTGTTTCTTTAAGGCACGCGGTGAATGCCGTTGTGAGCAA
				R	TCGAACCTGTGACCCGCGGGGGCCAACAACGTGCAGCACTTCTAGAAGGCACGACGGGAACACCGC

					TTCCTTACTAT
miR-328-3p	180	GGCUACGUAGCUCAGUUGGUUAGAGCAGCGGCCGGGCCAGCUGUGAGUGUUUCUUCUGGCCCUCUCUGCCCUUCCGUUGUGAGCAAUAGUAAGGAAGCGGGGGGGGAGAUGGGGGCCAUUAGAAGUGCUGCACGUUGUUGGCCCCCGCGGGUCACAGGUUCGAAUCCCGUCGUAGCCACCA	58,335	F	GTTAGAGCAGCGGCCGGGCCAGCTGTGAGTGTTTCTTCTGGCCCTCTCTGCCCTTCCGTTGTGAGCAATAGTAA
				R	TCGAACCTGTGACCCGCGGGGGCCAACAACGTGCAGCACTTCTAATGGCCCCCATCTCCCCCCCGCTTCCTTACTATTGC
anti-miR-451b-5p	180	GGCUACGUAGCUCAGUUGGUUAGAGCAGCGGCCGGGCCAGCUGUGAGUGUUUCUUCCGUUCCUUUGGCAAUGGUAAUUGUGAGCAAUAGUAAGGAAAUUACCAUUCCAUAAGGAACGUUAGAAGUGCUGCACGUUGUUGGCCCCCGCGGGUCACAGGUUCGAAUCCCGUCGUAGCCACCA	58,156	F	GTTAGAGCAGCGGCCGGGCCAGCTGTGAGTGTTTCTTCCGTTCCTTTGGCAATGGTAATTGTGAGCAATAGTA
				R	TCGAACCTGTGACCCGCGGGGGCCAACAACGTGCAGCACTTCTAACGTTCCTTATGGAATGGTAATTTCCTTACTA
$tRNA_{Met}$	75	GGCUACGUAGCUCAGUUGGUUAGAGCAGCGGCCGAUAUCCGCGGGUCACAGGUUCGAAUCCCGUCGUAGCCACCA	24,344	F	TTGTAACGCTGAATTCGGCTACGTAGCTCAGTTGGTTAGAGCAGCGGCCGATATCCGCGGGTCACAGGT
				R	CTTTCGCTAAGGATCTGCAGTGGTGGCTACGACGGGATTCGAACCTGTGACCCGCGGATAT
MSA	107	GGCUACGUAGCUCAGUUGGUUAGAGCAGCGGCCGAGUAAUUUACGUCGACGGGUGACGUCGAUGGGUUGCGGCCGCGGGUCACAGGUUCGAAUCCCGUCGUAGCCACCACUGCAGAUCCUUAGCGAAAGCUAAGGAUUUUUUUUAAGCUU	47,870		
miR-206-3p	180	GGCUACGUAGCUCAGUUGGUUAGAGCAGCGGCCGGGCCAGCUGUGAGUGUUUCUUUGGAAUGUAAGGAAGUGUGUGGUGUGAGCAAUAGUAAGGAACCACAUGCUUCUUUAUAUCCCCAAGAAGUGCUGCACGUUGUUGGCCCCCGCGGGUCACAGGUUCGAAUCCCGUCGUAGCCACCA	58,251	F	GTTAGAGCAGCGGCCGGGCCAGCTGTGAGTGTTTCTTTGGAATGTAAGGAAGTGTGTGGTGTGAGCAA
				R	TCGAACCTGTGACCCGCGGGGGCCAACAACGTGCAGCACTTCTTGGGGATATAAAGAAGCATGTGGTTCCTTACTA
anti-miR-21-5p-3	180	GGCUACGUAGCUCAGUUGGUUAGAGCAGCGGCCGGGCCAGCUGUGAGUGUUUCUUGACUGGUGUUGCCAUGAGAUUUUGUGAGCAAUAGUAAGGAAGAAUCUCAUGCAUACACCAGUAUAGAAGUGCUGCACGUUGUUGGCCCCCGCGGGUCACAGGUUCGAAUCCCGUCGUAGCCACCA	58,235	F	GTTAGAGCAGCGGCCGGGCCAGCTGTGAGTGTTTCTTGACTGGTGTTGCCATGAGATTTTGTGAGCAATA
				R	TCGAACCTGTGACCCGCGGGGGCCAACAACGTGCAGCACTTCTATACTGGTGTATGCATGAGATTCTTCCTTAC
miR-33a-5p	180	GGCUACGUAGCUCAGUUGGUUAGAGCAGCGGCCGGGCCAGCUGUGAGUGUUUCUUGUGCAUUGUAGUUGCAUUGCAUUGUGAGCAAUAGUAAGGAAGGUGCAAUGAAACGACAAUGCAAAGAAGUGCUGCACGUUGUUGGCCCCCGCGGGUCACAGGUUCGAAUCCCGUCGUAGCCACCA	58,361	F	GTTAGAGCAGCGGCCGGGCCAGCTGTGAGTGTTTCTTGTGCATTGTAGTTGCATTGCATTGTGAGCAAT
				R	TCGAACCTGTGACCCGCGGGGGCCAACAACGTGCAGCACTTCTTTGCATTGTCGTTTCATTGCACCTTCCTTACT

miR-130b-3p	180	GGCUACGUAGCUCAGUUGGUUAGAGCAGCGGCCGGGCCAGCUGUGAGUGUUUCUUCAGUGCAAUGAUGAAAGGGCAUUGUGAGCAAUAGUAAGGAAGUGCUCUUUCCCCGUUGCACUAUAGAAGUGCUGCACGUUGUUGGCCCCCGCGGGUCACAGGUUCGAAUCCCGUCGUAGCCACCA	58,226	F	GTTAGAGCAGCGGCCGGGCCAGCTGTGAGTGTTTCTTCAGTGCAATGATGAAAGGGCATTGTGAGCAATAGTAA
				R	TCGAACCTGTGACCCGCGGGGGCCAACAACGTGCAGCACTTCTATAGTGCAACAGGGAAAGAGCACTTCCTTACTATTGC
anti-miR-21-5p-2	180	GGCUACGUAGCUCAGUUGGUUAGAGCAGCGGCCGGGCCAGCUGUGAGUGUUUCUUGAUUCAACAGUCAACAUCAGUCUGUGAGCAAUAGUAAGGAAGACUGAUGUGACUUGUUGAAUAUAGAAGUGCUGCACGUUGUUGGCCCCCGCGGGUCACAGGUUCGAAUCCCGUCGUAGCCACCA	58,243	F	GTTAGAGCAGCGGCCGGGCCAGCTGTGAGTGTTTCTTGATTCAACAGTCAACATCAGTCTGTGAGCAATAGT
				R	TCGAACCTGTGACCCGCGGGGGCCAACAACGTGCAGCACTTCTATATTCAACAAGTCACATCAGTCTTCCTTAC
anti-miR-122-5p	180	GGCUACGUAGCUCAGUUGGUUAGAGCAGCGGCCGGGCCAGCUGUGAGUGUUUCUUUUACCACAAACACAGAUUUGAUUGUGAGCAAUAGUAAGGAAAUCAAAUCUUGUCUUGUGGUACUAGAAGUGCUGCACGUUGUUGGCCCCCGCGGGUCACAGGUUCGAAUCCCGUCGUAGCCACCA	58,125	F	GTTAGAGCAGCGGCCGGGCCAGCTGTGAGTGTTTCTTTTACCACAAACACAGATTTGATTGTGAGCAATAGTA
				R	TCGAACCTGTGACCCGCGGGGGCCAACAACGTGCAGCACTTCTAGTACCACAAGACAAGATTTGATTTCCTTACTA
scrm-5	180	GGCUACGUAGCUCAGUUGGUUAGAGCAGCGGCCGGGCCAGCUGUGAGUGUUUCUUGGUGUCGUUUCUCUGGUGAGUAUGUGAGCAAUAGUAAGGAAGUACUCACCAUAGAAACGACACAAGAAGUGCUGCACGUUGUUGGCCCCCGCGGGUCACAGGUUCGAAUCCCGUCGUAGCCACCA	58,273	F	GTTAGAGCAGCGGCCGGGCCAGCTGTGAGTGTTTCTTGGTGTCGTTTCTCTGGTGAGTATGTGAGCAAT
				R	TCGAACCTGTGACCCGCGGGGGCCAACAACGTGCAGCACTTCTTGTGTCGTTTCTATGGTGAGTACTTCCTTACTA
scrm-4	180	GGCUACGUAGCUCAGUUGGUUAGAGCAGCGGCCGGGCCAGCUGUGAGUGUUUCUUAAGCGCGCUUUGUAGGAUUCGUUGUGAGCAAUAGUAAGGAAGCGAAUCCUCAAUAGCGCGCUGUAGAAGUGCUGCACGUUGUUGGCCCCCGCGGGUCACAGGUUCGAAUCCCGUCGUAGCCACCA	58,281	F	GTTAGAGCAGCGGCCGGGCCAGCTGTGAGTGTTTCTTAAGCGCGCTTTGTAGGATTCGTTGTGAGCAA
				R	TCGAACCTGTGACCCGCGGGGGCCAACAACGTGCAGCACTTCTACAGCGCGCTATTGAGGATTCGCTTCCTTACTAT
scrm-2	180	GGCUACGUAGCUCAGUUGGUUAGAGCAGCGGCCGGGCCAGCUGUGAGUGUUUCUUGUUCGUCUGUAGACGGUUGUUGUGUGAGCAAUAGUAAGGAAGCAACAACCUUCUCCAGACGAAAAGAAGUGCUGCACGUUGUUGGCCCCCGCGGGUCACAGGUUCGAAUCCCGUCGUAGCCACCA	58,249	F	GTTAGAGCAGCGGCCGGGCCAGCTGTGAGTGTTTCTTGTTCGTCTGTAGACGGTTGTTGTGTGAGCAAT
				R	TCGAACCTGTGACCCGCGGGGGCCAACAACGTGCAGCACTTCTTTTCGTCTGGAGAAGGTTGTTGCTTCCTTACTA
scrm-3	180	GGCUACGUAGCUCAGUUGGUUAGAGCAGCGGCCGGGCCAGCUGUGAGUGUUUCUUUUCUCCGAAGCUGUCACGUUUUUGUGAGCAAUAGUAAGGAAGAAUCGUGUAGCUUUCGGAGACUAGAAGUGCUGCACGUUGUUGGCCCCCGCGGGUCACAGGUUCGAAUCCCGUCGUAGCCACCA	58,181	F	GTTAGAGCAGCGGCCGGGCCAGCTGTGAGTGTTTCTTTTCTCCGAAGCTGTCACGTTTTTGTGAGCAAT
				R	TCGAACCTGTGACCCGCGGGGGCCAACAACGTGCAGCACTTCTAGTCTCCGAAAGCTACACGATTCTTCCTTACTAT
scrm-1	180	GGCUACGUAGCUCAGUUGGUUAGAGCAGCGGCCGGGCCAGCUGUGAGUGUUUCUUGUGUAACACGUCUAUACGCCCAUGUGAGCAAU	58,335	F	GTTAGAGCAGCGGCCGGGCCAGCTGTGAGTGTTTCTTGTGTAACACGTCTATACGCCCATGTGAGCA

		AGUAAGGAAGUGGGCGUACAGAAGUGUUACAAAGAAGUGCUGCA CGUUGUUGGCCCCCGCGGGUCACAGGUUCGAAUCCCGUCGUAGC CACCA			A
				R	TCGAACCTGTGACCCGCGGGGGCCAACAACGTG CAGCACTTCTTTGTAACACTTCTGTACGCCCACTT CCTTACTATTG
miR-21-5p	180	GGCUACGUAGCUCAGUUGGUUAGAGCAGCGGCCGGGCCAGCUG UGAGUGUUUCUUUAGCUUAUCAGACUGAUGUUGAUGUGAGCAAU AGUAAGGAAGUCAACAUCCGUCGAUGGGCUGUAGAAGUGCUGCA CGUUGUUGGCCCCCGCGGGUCACAGGUUCGAAUCCCGUCGUAGC CACCA	58,267	F	GTTAGAGCAGCGGCCGGGCCAGCTGTGAGTGTT TCTTTAGCTTATCAGACTGATGTTGATGTGAGCAA T
				R	TCGAACCTGTGACCCGCGGGGGCCAACAACGTG CAGCACTTCTACAGCCCATCGACGGATGTTGACT TCCTTACTA
anti-miR-21-5p	180	GGCUACGUAGCUCAGUUGGUUAGAGCAGCGGCCGGGCCAGCUG UGAGUGUUUCUUUCAACAUCAGUCUGAUAAGCUAUGUGAGCAAUA GUAAGGAAGUAGCUUAUAAGAAUGAUGUUGCAGAAGUGCUGCAC GUUGUUGGCCCCCGCGGGUCACAGGUUCGAAUCCCGUCGUAGCC ACCA	58,267	F	GTTAGAGCAGCGGCCGGGCCAGCTGTGAGTGTT TCTTTCAACATCAGTCTGATAAGCTATGTGAGCAA
				R	TCGAACCTGTGACCCGCGGGGGCCAACAACGTG CAGCACTTCTGCAACATCATTCTTATAAGCTACTT CCTTACTA
miR-34a/ TPA3'	213	GGCUACGUAGCUCAGUUGGUUAGAGCAGCGGCCGGGCCAGCUG UGAGUGUUUCUUUGGCAGUGUCUUAGCUGGUUGUUGUGAGCAAU AGUAAGGAAGCAAUCAGCAAGUAUACUGCCCUAGAAGUGCUGCAC GUUGUUGGCCCGGCGAUACCAGCCGAAAGGCCCUUGGCAGCGUC CCGCGGGUCACAGGUUCGAAUCCCGUCGUAGCCACCA	68,926	F	GTTAGAGCAGCGGCCGGGCCAGCTGTGAGTGTT TCT
				R	TCGAACCTGTGACCCGCGGGACGCTGCCAAGGG CCTTTCGGCTGGTATCGCCGGGCCAACAACGTG CAGC
miR-34a/ TPA3'+ TPA5'	246	GGCUACGUAGCUCAGUUGGUUAGAGCAGCGGCCGGGCGATACCA GCCGAAAGGCCCUUGGCAGCGUCGGCCAGCUGUGAGUGUUUCUU UGGCAGUGUCUUAGCUGGUUGUUGUGAGCAAUAGUAAGGAAGCA AUCAGCAAGUAUACUGCCCUAGAAGUGCUGCACGUUGUUGGCCC GGCGAUACCAGCCGAAAGGCCCUUGGCAGCGUCCCGCGGGUCAC AGGUUCGAAUCCCGUCGUAGCCACCA	79,610	F	GTTAGAGCAGCGGCCGGGCGATACCAGCCGAAA GGCCCTTGGCAGCGTCGGCCAGCTGTGAGTGTT T
				R	TCGAACCTGTGACCCGCGGGACGCTGCCAAGGG CCTTTCGGCTGGTATCGCCGGGCCAACAACGTG CAGC
miR-888/ pegaptanib3'	207	GGCUACGUAGCUCAGUUGGUUAGAGCAGCGGCCGGGCCAGCUG UGAGUGUUUCUUUACUCAAAAAGCUGUCAGUCAUUGUGAGCAAUA GUAAGGAAGUGACUGACGCUUUUUUGGGUCUAGAAGUGCUGCAC GUUGUUGGCCCCGGAAUCAGUGAAUGCUUAUACAUCCGCCGCGG GUCACAGGUUCGAAUCCCGUCGUAGCCACCA	66,868	F	GTTAGAGCAGCGGCCGGGCCAGCTGTGAGTGTT TCTTTACTCAAAAAGCTGTCAGTCATTGTGAGCAA TAGTAA
				R	TCGAACCTGTGACCCGCGGCGGATGTATAAGCAT TCACTGATTCCGGGGCCAACAACGTGCAGCACTT CTAGACCCAAAAAAGCGTCAGTCACTTCCTTACT ATTGC
miR-34a/ pegaptanib5'	207	GGCUACGUAGCUCAGUUGGUUAGAGCAGCGGCCGCGGAAUCAGU GAAUGCUUAUACAUCCGGGCCAGCUGUGAGUGUUUCUUUGGCAG UGUCUUAGCUGGUUGUUGUGAGCAAUAGUAAGGAAGCAAUCAGC AAGUAUACUGCCCUAGAAGUGCUGCACGUUGUUGGCCCCCGCGG GUCACAGGUUCGAAUCCCGUCGUAGCCACCA	66,922	F	GTTAGAGCAGCGGCCGCGGAATCAGTGAATGCT TATACATCCGGGCCAGCTGTGAGTGTTTCTTTGG CAGTGTCTTAGCTGGTTGTTGTGAGCAATAGTAA
				R	GCATTCACTGATTCCGCGGGGGCCAACAACGTG CAGCACTTCTAGGGCAGTATACTTGCTGATTGCT TCCTTACTATTGC
miR-34a/ EpCAM	199	GGCUACGUAGCUCAGUUGGUUAGAGCAGCGGCCGGGCCAGCUG UGAGUGUUUCUUUGGCAGUGUCUUAGCUGGUUGUUGUGAGCAAU AGUAAGGAAGCAAUCAGCAAGUAUACUGCCCUAGAAGUGCUGCAC	64,373	F	GTTAGAGCAGCGGCCGGGCCAGCTGTGAGTGTT TCT

A3'	GUUGUUGGCCCGCGACUGGUUACCCGGUCGCCGCGGGUCACAG GUUCGAAUCCCGUCGUAGCCACCA	R	TCGAACCTGTGACCCGCGGCGACCGGGTAACCA GTCGCGGGCCAACAACGTGCAGCAC

Supplemental Table 3. Yields and purities of nCAR/miR-34a-5p and nCAR/miR-124-3p isolated by single- and double-column-based, small-scale purification methods.

nCAR	Method	Yield (% of total RNA)	Yield (μg/mL bacterial culture)	Purity (%; by HPLC)
miR-34a-5p	Single-column	42.5	18.9	88.5%
	Double-column	33.0	14.8	97.8%
miR-124-3p	Single	44.3	15.4	94.8%
	Double	40.4	14.0	98.3%

Supplemental Table 4. Primers used for RT-qPCR analyses of miRNAs and mRNAs in this study.

Target		Primer Sequence
U6	Forward	5'-CTCGCTTCGGCAGCACA-3'
	Reverse	5'-AACGCTTCACGAATTTGCGT-3'
miR-34a	RT	5'-GTCGTATCCAGTGCAGGGTCCGAGGTATTCGCACTGGATACGACACAACC-3'
	Forward	5'-CGCGCTGGCAGTGTCTTAGCT-3'
	Reverse	5'-GTGCAGGGTCCGAGGT-3'
miR-124	RT	5'-GTCGTATCCAGTGCAGGGTCCGAGGTATTCGCACTGGATACGACGGCATT-3'
	Forward	5'-GCGCTAAGGCACGCGGTG-3'
	Reverse	5'-GTGCAGGGTCCGAGGT-3'
18S	Forward	5'-GTAACCCGTTGAACCCCATT-3'
	Reverse	5'-CCATCCAATCGGTAGTAGCG-3'
AMER1	Forward	5'-GCGAATTCGGAGACCCAAAAGGATGAAGCTGCTCAG-3′
	Reverse	5′-CCTTGCTCTTCCGGTGACGGCGGATACTGC-3
BAG2	Forward	5′-AGCCACATTAGGCGCTCGGTCT-3′
	Reverse	5′-AGTTAGAGGTTCGCGAGCCACACG-3′
BCL6B	Forward	5'-GCTTTGTACAGGTGGCACATC-3'
	Reverse	5'-GAACGTGGCTCTTGAGGGTC-3'
CLUH	Forward	5'-GGTAGCGGGCACGGTACA-3'
	Reverse	5'-GCATTGAGCACCCCAACAC-3'
GAS1	Forward	5'-CTGGGGTTTGTTACCAGTTG-3'
	Reverse	5'-GGGGGAAAGGTGTAATATGG-3'
IQGAP1	Forward	5'-GAAAGCCCAGGAAATCCAG-3'
	Reverse	5'-TCCATACAAGCCAACATCAG-3'
KCTD12	Forward	5'-GCTCGGGCTACATCACCATCGG-3'
	Reverse	5'-GGGTCCCGGCTTTCGTTCAG-3'
NECTIN1	Forward	5'-ACCAACCCCATCGGTACAC-3'
	Reverse	5'-GGGGTGTAGGGGAATTCTGT-3'
NID1	Forward	5'-CGGGGATGACTTCGTCTCTC-3′
	Reverse	5'-GTGGTGACGTAGACTGCGT-3′
NRAS	Forward	5'-CCTCTACAGGGAGCAGATTAAGCGA-3'
	Reverse	5'-CCCTGTCTGGTCTTGGCTGAGGT-3'
SNAI2	Forward	5'-TGGTTGCTTCAAGGACACAT-3'
	Reverse	5'-GCAGATGAGCCCTCAGATTT-3'
TMEM109	Forward	5'-ACACTGGATGCCTGGATTGGGC-3'
	Reverse	5'-AAGCCGAGGAGCAGAGACAGCA-3'
VAMP3	Forward	5'-GCAGCCAAGTTGAAGAGGAA-3'
	Reverse	5'-CAGTTTTGAGTTCCGCTGGT-3'
VIM	Forward	5'-GAGAACTTTGCCGTTGAAGC-3'
	Reverse	5'-TCCAGCAGCTTCCTGTAGGT-3'

References

Chen, Q. X., W. P. Wang, S. Zeng, S. Urayama and A. M. Yu (2015). A general approach to high-yield biosynthesis of chimeric RNAs bearing various types of functional small RNAs for broad applications. *Nucleic Acids Res* **43**: 3857-3869.

Feinstein, E. (2013). Oligoribonucleotide inhibitors of Nrf2 and methods of use thereof for treatment of cancer. *U.S. Patent:* **8410069**: B2.

Liu, C., W. Lou, Y. Zhu, N. Nadiminty, C. T. Schwartz, C. P. Evans and A. C. Gao (2014). Niclosamide inhibits androgen receptor variants expression and overcomes enzalutamide resistance in castration-resistant prostate cancer. *Clin Cancer Res* **20**: 3198-3210.

Luan, S., L. Sun and F. Huang (2010). MicroRNA-34a: a novel tumor suppressor in p53-mutant glioma cell line U251. *Arch Med Res* **41**: 67-74.

Miner, P., M. Wedel, B. Bane and J. Bradley (2004). An enema formulation of alicaforsen, an antisense inhibitor of intercellular adhesion molecule-1, in the treatment of chronic, unremitting pouchitis. *Alimentary Pharmacology and Therapeutics* **19**: 281-286.

Nakatsu, Y., X. Ma, F. Seki, T. Suzuki, M. Iwasaki, Y. Yanagi, K. Komase and M. Takeda (2013). Intracellular Transport of the Measles Virus Ribonucleoprotein Complex Is Mediated by Rab11A-Positive Recycling Endosomes and Drives Virus Release from the Apical Membrane of Polarized Epithelial Cells. *J Virol.* **87**: 4683-4693.

Ng, E. W., D. T. Shima, P. Calias, E. T. Cunningham, Jr., D. R. Guyer and A. P. Adamis (2006). Pegaptanib, a targeted anti-VEGF aptamer for ocular vascular disease. *Nat Rev Drug Discov* **5**: 123-132.

Raal, F. J., R. D. Santos, D. J. Blom, A. D. Marais, M. Charng, W. C. Cromwell, R. H. Lachmann, D. Gaudet, J. L. Tan, S. Chasan-Taber, D. L. Tribble, J. D. Flaim and S. T. Crooke (2010). Mipomersen, an apolipoprotein B synthesis inhibitor, for lowering of LDL cholesterol concentrations in patients with homozygous familial hypercholesterolaemia: a randomised, double-blind, placebo-controlled trial. *Lancet* **375**: 998-1006.

Schober, A., M. Nazari-Jahantigh, Y. Wei, K. Bidzhekov, F. Gremse, J. Grommes, R. T. Megens, K. Heyll, H. Noels, M. Hristov, S. Wang, F. Kiessling, E. N. Olson and C. Weber (2014). MicroRNA-126-5p promotes endothelial proliferation and limits atherosclerosis by suppressing Dlk1. *Nat Med* **20**: 368-376.

Shigdar, S., J. Lin, Y. Yu, M. Pastuovic, M. Wei and W. Duan (2011). RNA aptamer against a cancer stem cell marker epithelial cell adhesion molecule. *Cancer Sci* **102**: 991-998.

Zimmermann, G. R., C. L. Wick, T. P. Shields, R. D. Jenison and A. Pardi (2000). Molecular interactions and metal binding in the theophylline-binding core of an RNA aptamer. *RNA* **6**: 659-667.